AD-A079 635 HUGHES AIRCRAFT CO LOS ANGELES CALIF SPACE AND COMMU--ETC F/G 10/2
HIGH EFFICIENCY SOLAR PANEL, PHASE II, GALLIUM ARSENIDE,(U)
JUL 79 G VENDURA, S KAMATH, G WOLFE F33615-77-C-3150
UNCLASSIFIED HAC-SCG-90324M AFAPL-TR-79-2058 NL

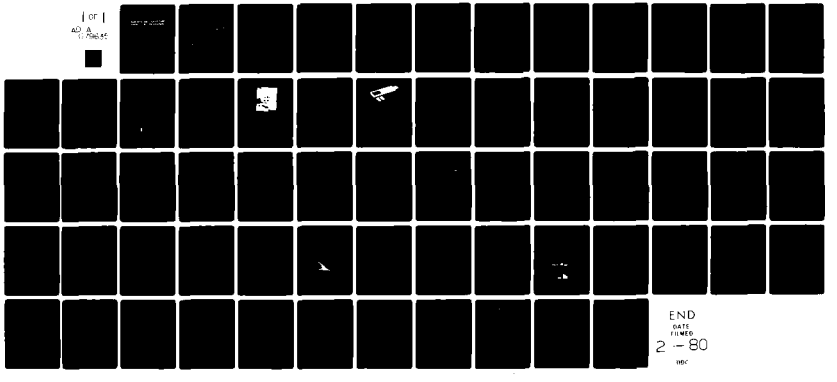

END
DATE FILMED
2-80
DDC

AFAPL-TR-79-2068

HIGH EFFICIENCY SOLAR PANEL, PHASE II, GALLIUM ARSENIDE

Interim Report for Period Covering September 1977 — January 1979

Prepared By:
Hughes Aircraft Company
Space and Communications Group
P.O. Box 92426
Los Angeles, California 90009

JULY 1979

TECHNICAL REPORT AFAPL-TR-79-2068

CONTRACT NO. F33615-77-C-3150

Approved for Public Release, Distribution Unlimited

Prepared For:
Air Force Aero Propulsion Laboratory
Air Force Wright Aeronautical Laboratories
Air Force Systems Command
Wright Patterson Air Force Base, Ohio 45433

NOTICE

When Government drawings, specifications, or other data are used for any purpose other than in connection with a definitely related Government procurement operation, the United States Government thereby incurs no responsibility nor any obligation whatsoever; and the fact that the government may have formulated, furnished, or in any way supplied the said drawings, specifications, or other data, is not to be regarded by implication or otherwise as in any manner licensing the holder or any person or corporation, or conveying any rights or permission to manufacture, use, or sell any patented invention that may in any way be related thereto.

This report has been reviewed by the Information Office (OI) and is releasable to the National Technical Information Service (NTIS). At NTIS, it will be available to the general public, including foreign nations.

This technical report has been reviewed and is approved for publication.

JERRY E. BEAM
Energy Conversion Branch

JOSEPH F. WISE
Technical Area Manager
Energy Conversion Branch

FOR THE COMMANDER

JAMES D. REAMS
Chief, Aerospace Power Division

"If your address has changed, if you wish to be removed from our mailing list, or if the addressee is no longer employed by your organization please notify AFAPL POE, W-PAFB, OH 45433 to help us maintain a current mailing list."

Copies of this report should not be returned unless return is required by security considerations, contractual obligations, or notice on a specific document.

UNCLASSIFIED

SECURITY CLASSIFICATION OF THIS PAGE (When Data Entered)

REPORT DOCUMENTATION PAGE	READ INSTRUCTIONS BEFORE COMPLETING FORM
1. REPORT NUMBER: AFAPL-TR-79-2058 (Panel)	2. GOVT ACCESSION NO. / 3. RECIPIENT'S CATALOG NUMBER
4. TITLE (and Subtitle): High Efficiency Solar Panel Phase II, Gallium Arsenide.	5. TYPE OF REPORT & PERIOD COVERED: Interim Report, 15 Sept 77 – Sept 77 – Jan 79 / 15 Jan 79
	6. PERFORMING ORG. REPORT NUMBER: SCG-90324M (Ref E0773)
7. AUTHOR(s): G. Vendura, S. Kamath, G. Wolff	8. CONTRACT OR GRANT NUMBER(s): F33615-77-C-3150
9. PERFORMING ORGANIZATION NAME AND ADDRESS: Hughes Aircraft Co. Space & Communications Group P.O. Box 92919, Los Angeles CA 90009	10. PROGRAM ELEMENT, PROJECT, TASK AREA & WORK UNIT NUMBERS: PE 62203F, Proj 68 Task 682J04 W.U. 6825 / 682J / 04
11. CONTROLLING OFFICE NAME AND ADDRESS: Air Force Aero Propulsion Laboratory POE-2 Wright-Patterson AFB, OH 45433	12. REPORT DATE: July 1979
	13. NUMBER OF PAGES: 60
14. MONITORING AGENCY NAME & ADDRESS (if different from Controlling Office)	15. SECURITY CLASS. (of this report): UNCLASSIFIED
	15a. DECLASSIFICATION/DOWNGRADING SCHEDULE
16. DISTRIBUTION STATEMENT (of this Report): Approved for public release Distribution unlimited / HAC-SCG-90324M, HAC-REF-E0773	
17. DISTRIBUTION STATEMENT (of the abstract entered in Block 20, if different from Report)	
18. SUPPLEMENTARY NOTES	
19. KEY WORDS (Continue on reverse side if necessary and identify by block number): GaAs solar cells, space power, solar energy conversion	

20. ABSTRACT (Continue on reverse side if necessary and identify by block number)

This interim report presents the progress of the GaAs High Efficiency Solar Panel program (Phase II) goal of development of space qualified solar cells of 16 percent efficiency AMO during the period of September 1977 through January 1979. Results of developmental research involving the basic GaAs substrate, epitaxial reactors, LPE growth processes, ohmic contacts/metallizations, welding capability, and environmental testing are included. Efforts to increase substrate size and fabrication yield to enhance the feasibility of larger scale GaAs solar cell production are also detailed.

DD FORM 1 JAN 73 1473

UNCLASSIFIED

SECURITY CLASSIFICATION OF THIS PAGE (When Data Entered)

391 903 LB

PREFACE

This interim report presents the progress of the GaAs High Efficiency Solar Panel program (Phase II) goal of development of space qualified solar cells of 16 percent efficiency AMO during the period of September 1977 through January 1979. Results of development research involving the basic GaAs substrate, the epitaxial reactors, LPE growth processes, ohmic contacts/metallizations, welding capability, and environmental testing are included. Efforts to increase substrate size and fabrication yield to enhance the feasibility of larger scale GaAs solar cell production are also detailed.

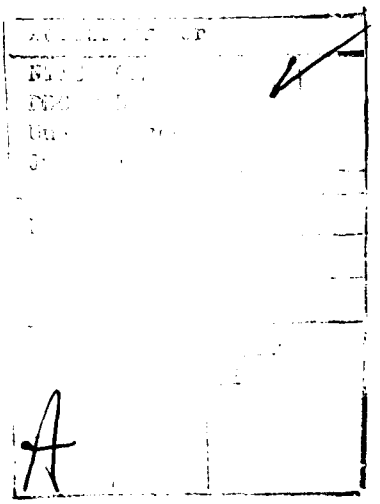

TABLE OF CONTENTS

LIST OF ILLUSTRATIONS

LIST OF TABLES

1. INTRODUCTION

1.1 Program Objectives. This report covers the work done during the period of 15 September 1977 to 15 January 1979 by Hughes Aircraft Company on GaAs solar cells for the High Efficiency Solar Panel (HESP), Phase II (Contract F33615-77-C-3150).

The objective of this program is the development of space qualified solar cells having a beginning of life lot median efficiency of 16 percent at 25°C under air mass zero (AM0) illumination. The solar cell assembly must withstand both laser and nuclear weapons effects as well as the natural space environment at synchronous earth orbit. Also, the cells must be readily producible in large quantities.

The end results of the program are high efficiency GaAs solar cells capable of being produced in large quantities; documentation of the qualification testing performed on the cells; a process identification document describing the cell production processes, documentation of facility, material, and personnel requirements for sustained high volume production; and trained production engineering personnel who can assume responsibility for any subsequent high volume production.

1.2 Program Status. During the year the fabrication of 2 x 2 cm GaAs cells has been firmly established using a reliable and reproducible process sequence capable of yielding finished cells with an AM0 efficiency of 16 percent. In addition, preliminary documentation of the process has been completed. These cells have been subjected to temperature extremes between -195° and 300°C with no deleterious effects, and the suitability of the contacts for welding has been demonstrated.

Through the growth of numerous batches of such cells to date under the contract, characteristics have gradually improved and the fabrication yield has steadily increased. Present yield for 15 percent efficient cells is 60 percent while that for 16 percent is about 50 percent.

2. PROGRAM PLAN

2.1 Schedule. The program schedule is shown in Figure 1 and outlines specific tasks or milestones. These, in turn, can be roughly divided into three major categories:

1) Development

2) Manufacturing control/qualification testing

3) Delivery

The first of these tasks involves extensive research and development of the basic GaAs cell over a period of 12 to 15 months. This in turn requires preliminary testing to ensure proper characteristics. For instance, contacts to cells are required to be low resistance, ohmic, weldable, and capable of meeting the contract's high temperature specifications, and the cells must exhibit significant radiation hardness and be capable of withstanding specific temperature extremes. During this stage of the contract, fabrication processes are often significantly altered a number of different times in order to design into the cell itself the required behavior and qualities.

The second period involving manufacturing control and qualification testing lasts about 6 months and entails freezing all fabrication processes. At this point, the cell becomes sufficiently standardized so that finished devices are as close to identical as possible. This standardization process is followed by elaborate qualification testing covering all aspects of the finalized solar cell design. Test criteria include electrical, mechanical, radiation, and thermal suitability. In addition, the effects or characteristics of the cover glass, the antireflection coating, and the contacts and interconnects are examined.

After manufacturing control documentation and qualification testing are completed, the final delivery phase of the contract is entered upon during which larger quantities of individual cells are fabricated in accordance with the processes developed during the earlier stages. For delivery these cells either remain separate or are interconnected into modules as required by the contract. During this stage, some large and some thin GaAs cells are also expected to be fabricated.

2.2 Baseline Design. The basic GaAs cell structure, shown in Figure 2, consists of a highly doped (Te) n^+ substrate upon which two separate layers are deposited. The first layer is a 10 μm (Sn) n type buffer upon which a

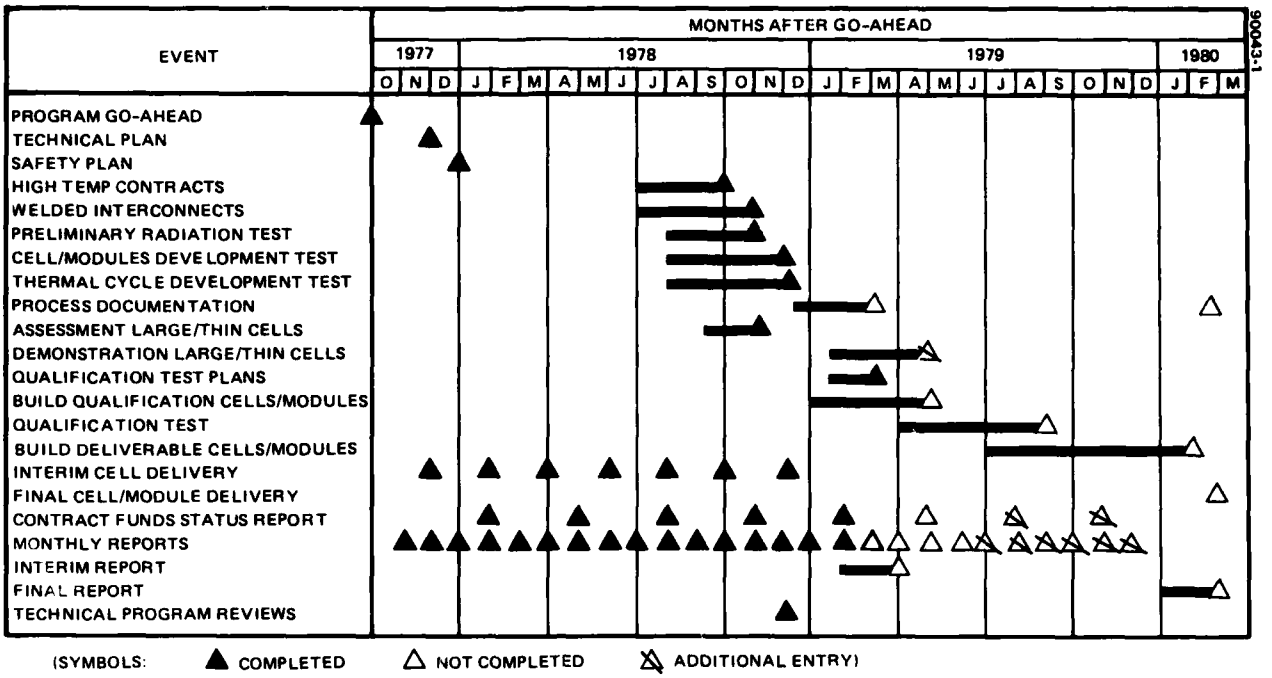

Figure 1. GaAs HESP II program schedule (September 15, 1977 to February 15, 1980).

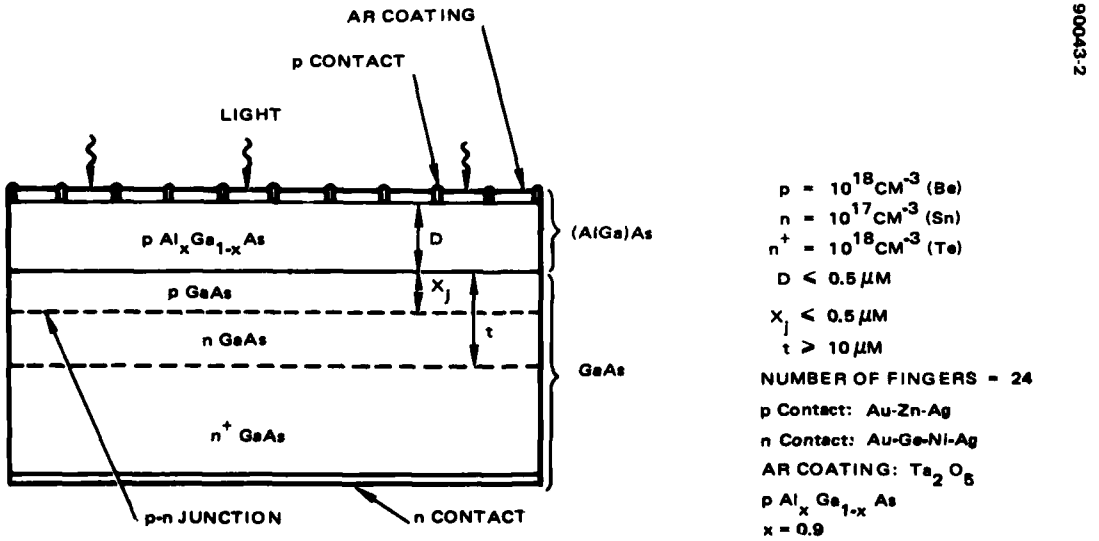

Figure 2. GaAs solar cell baseline design.

0.5 μm p (AlGa)As window is grown. The actual junction is formed by diffusion of Be dopant from the window into the buffer layer. The p GaAs thickness (junction depth, x_j) is an extremely important parameter for radiation damage control and is therefore crucial to space cell performance.

The basic solar cell structure is further detailed in the specifications listed in Tables 1 through 3. As shown, the AuZn p contacts are about 2000 Å with a silver overlay of about 5 μm thick, and the n contact is AuGeNi (~2000 Å) with a similar Ag overlay. The antireflection coating is Ta_2O_5, the thickness of which has been optimized to match the spectral response of the GaAs cell.

TABLE 1. GaAs HESP II SOLAR CELL PHYSICAL SPECIFICATIONS

Cell size	
Length	0.79 in
Width	0.79 in
Height	0.030 in (with cover glass) 0.012 in (without cover glass)
Cell area	
Total	0.620 in^2
Active	0.562 in^2
Cell weight	
Without cover	0.67 gm
With cover	0.91 gm
Upper contact	
Number of gridlines	24 lines
Gridline length	0.74 in
Gridline width	0.0024 in
Contact bar length	0.753 in
Contact bar width	0.31 in
Gridline total thickness	~6.0 μm
Lower contact	
Length	0.79 in
Width	0.79 in
Area	0.620 in^2
Total thickness	~6.0 μm
Cover glass	
Length	0.77 in
Width	0.80 in
Area	0.616 in^2
Thickness	0.012 in

TABLE 2. GaAs HESP II SOLAR CELL MATERIAL SPECIFICATIONS

Cell material	GaAs
Substrate	
Orientation	100
Type	n^+
Dopant	Te
Concentration	7×10^{17} cm^{-3}
Thickness	0.015 in.
First epilayer	
Type	n
Dopant	Sn
Concentration	1×10^{17} cm^{-3}
Thickness	10 μm
Resistivity	0.014 Ω-cm
Second epilayer	
Type	p
Dopant	Be
Concentration	1×10^{18} cm^{-3}
Thickness	<0.5 μm
Window layer	
Composition	(AlGa) As
Type	p^+
Dopant	Be
Concentration	1×10^{18} cm^{-3}
Thickness	<0.5 μm
Sheet resistance	0.03 Ω-cm
Junction depth	<0.5 μm
Upper surface	
First metallization	
Metals	AuZn
Thickness	2000 Å
Second metallization	
Metal	Ag
Thickness	5.0 μm
Cover glass adhesive	Dow Corning DC 93-500
Antireflection coating	
Material	Ta_2O_5
Length	0.77 in.
Width	0.79 in.
Thickness	750 Å
Lower surface	
First metallization	
Metals	AuGeNi
Thickness	2000 Å
Second metallization	
Metal	Ag
Thickness	5.0 μm
Cover glass	
Material	Corning 7940 - fused silica
Length	0.77 in.
Width	0.80 in.
Thickness	0.012 in.
AR coating (on top of glass)	MgF_2

TABLE 3. GaAs HESP II SOLAR CELL ELECTRICAL SPECIFICATIONS*

I_{sc} (short circuit current)	114 mA
V_{oc} (open circuit voltage)	1.00 V
I_{mp}	102 mA
V_{mp}	0.85 V
P_{max} (maximum power)	86.5 mW (4 cm^2)
Energy conversion efficiency	16.0%

*Average values.

2.3 Overview. As stated earlier, the main HESP II objective is a 16 percent efficient cell that is as production ready as possible. This objective necessitated further development of the basic GaAs solar cell itself which involved continual periodic testing.

Of central importance was the growth of the GaAs buffer and window layers which, in turn, determine the depth of the junction. For this determination, control of not only the solution characteristics is most critical but also the delicate temperature and time dependency maintained during the growth procedure. In Section 3, details of the liquid phase epitaxy (LPE) process are presented along with resulting progress with respect to cells fabricated by this technique.

Another key element involves the metallizations applied to the GaAs cell. This phase of the program can actually be broken down into two parts: contacts and interconnect methods.

The former concerns the layer or layers of metals deposited on both the p type and n type cell surfaces. Ideally, such contacts must have excellent mechanical strength as well as low electrical resistance. An additional criterion, stipulated by the HESP II contract, is specific high temperature survivability. Interconnect methods, on the other hand, address the task of applying connectors onto the various contact metallizations for subsequent building of cells into arrays. For HESP II, the feasibility of ultrasonic seam welding tabs was studied. Areas of interest include the electrical characteristics of individual cells after the welding operation as well as the mechanical strength of the resulting bonds. Details of both the contact metallizations and the interconnecting method are given in Section 4.

Since a critical goal of the HESP II program was production readiness, ways were investigated to minimize the costs associated with cell fabrication. As a result, attention was centered on the substrate cell geometry. Relatively large area rectangular GaAs substrates are desirable so that more than one cell can be made on a single substrate during any single liquid phase epitaxy growth process. The rectangular shape is useful in order to reduce to a minimum losses due to excess material cut away when the rectangular cell is cleaved from the processed substrates. Section 5 outlines the most economical way to grow such substrates – a way which involved extensive

experimentation of various boat materials. This study, in turn, expanded into a search for suitable boat liners and both new growth and slicing orientations.

In the same section results are given of the attempt to reduce the initial thickness of the GaAs substrate in an effort to eventually minimize both the cost and overall weight of the individual cell. This effort involved not merely slicing single crystal ingots into thinner substrates but doing so in a speedy, economical fashion with respectable yields. The study therefore expanded into a comparison of two different sectioning methods involving both inner diameter (ID) and multiblade saws. In addition, postsaw processing (involving mechanical grinding, chemical etching, and handling) becomes significant for complete assessment of fabrication breakage and for the establishment of the ultimate yield figures.

Certain test results are implicit with respect to the various aspects of the program already briefly outlined. For instance, associated with cell fabrication are the results of numerous current-voltage characteristics exhibiting efficiency, open circuit voltage and other parameters, and the welding study involves electrical and tab pull data. Other cell tests, however, do not fall so squarely into the categories already described and are massed separately in Section 6. In general, these include individual developmental and environmental studies that can be divided into the following subcategories:

1) Temperature cycling

2) Temperature-humidity

3) High temperature contacts

4) Radiation

5) Welding

Finally, in Section 7 concluding remarks are made in which the present status of the contract is summarized, and an outline of future effort is made. In particular, the importance of the manufacturing control documentation and qualification test tasks is discussed at length.

3. GaAs CELL PROCESSES

3.1 GaAs Growth Method. A key element in the success of the GaAs solar cell program is the novel technology developed at Hughes Aircraft Company to grow large area GaAs and (AlGa)As layers reproducibly using infinite solution liquid phase epitaxy (LPE).

A schematic of the apparatus is shown in Figure 3. It features an all quartz growth tube connected to a stainless steel entry chamber through a high vacuum valve. A solution of high purity GaAs in either Ga or a mixture of Ga and Al serves as the growth solution. The Al:Ga ratio can be adjusted to give any composition from GaAs to AlAs for the epitaxial layer, and dopants such as Te, Sn, Ge, or Be can be used to produce a variety of doped layers. Once a solution is prepared, it is maintained in a pure Pt crucible under a diffused hydrogen ambient at close to the growth temperature for long periods while layers are grown.

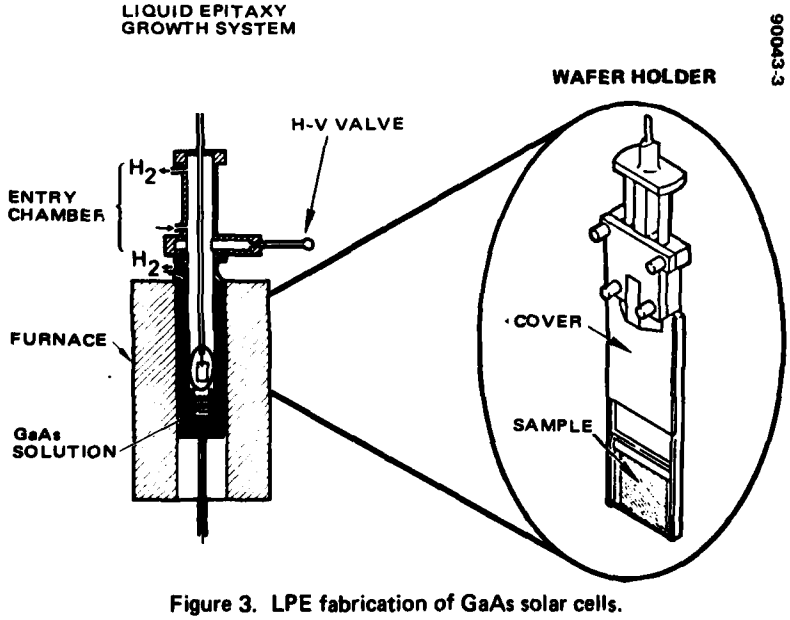

Figure 3. LPE fabrication of GaAs solar cells.

Layers have been reproducibly grown from the system with thicknesses down to 0.5 μm with a variation in thickness of less than ±10 percent over substrates larger than 6 cm^2 in area. The surfaces are specular and can be processed as grown for devices. Since a growth run takes only about an hour, the system can be adapted for large scale production of low cost cells.

A substrate holder (Figure 3) fabricated from graphite is used to ensure good equilibration between the substrate and the growth solution prior to the start of growth. It enhances the capability of the infinite solution system for the growth of strain-free, large-area layers with a uniformity in carrier concentration and thickness that would be difficult without it.

The advantages of this technique stem from the use of a large, stable solution that permits the growth of epitaxial layers even for several years. This results in efficient use of gallium under extremely safe and reliable conditions. Measurements of cells fabricated under the HESP II program have attested to the success of the process. By modifying the graphite substrate holder it will be possible for the method to be adapted for the growth of 32 GaAs cells (2 x 2 cm) in a single epitaxial run in a total growth cycle time of less than 2 hours. Additionally, it has also been demonstrated in an early phase of HESP II that the infinite solution technique can be used to tailor the cell parameters to yield a structure with very good control over both the window (AlGa)As layer thickness and the junction depth.

The cell characteristics have been measured in a large number of cases to prove that other relevant parameters that control the cell performance are well within the operational control of the technique. These parameters include the (AlGa)As window layer composition, thicknesses, and doping levels as well as the interface behavior in the solar cell structure.

3.2 Epitaxial Process Development. The infinite solution epitaxial growth technique was chosen from several alternatives to produce the solar cell structure because of the quality of the resulting GaAs and (AlGa)As layers and because it is by far the most economical and best developed process presently available. On the other hand, since the HESP II objective is large scale production of the cells, it was felt that the growth system had to be modified to permit the epitaxial growth of several substrates simultaneously.

The first step in this direction was taken in the early part of the program when the graphite substrate holder was modified to handle not a single substrate, but, instead, one substrate on either side of the holder. In addition, the LPE growth system itself was increased in size to hold a 3000 gm solution of GaAs in order to allow production of LPE layers in greater numbers. This system, shown in Figure 4, was checked out during a series of runs in which the layers grown using two substrates per holder were examined to determine both reproducibility and thickness uniformity. The results of these early tests led to modifications of the temperature profiles in the epitaxial reactor as

Figure 4. Hughes infinite solution epitaxy system with 3000 gram capacity (Photo M12175).

well as to the determination of the proper cooling rates needed to permit the growth of 0.5 μm window layers within a period of 2 to 5 minutes. The time was carefully chosen to be long enough to provide sufficient leeway for the system to attain reproducible conditions during growth but at the same time short enough to reduce machine cycle time so as to minimize cost. In addition, mechanical tolerances in the substrate holder construction had to be tightened to increase the layer uniformity, and the temperature controls had to be refined by the use of a microprocessor that could control the temperature by a multistep program during the loading of the substrates and their introduction into the solution. With these modifications, it is possible to obtain extremely similar solar cell characteristics for the cells grown in each run and reproducible characteristics from run to run. This is demonstrated in Tables 4 through 6, each of which shows the electrical parameters of cells grown together in individual runs but at different stages of the present contract. Notably, the reproducibility of cells within each run is excellent, while the overall quality of cells from run to run shows steady improvement.

TABLE 4. CHARACTERISTICS OF EARLY GaAs SOLAR CELLS GROWN IN SUCCESSIVE LPE RUNS IN DECEMBER 1977

Cell No.	I_{sc}, (mA)	V_{oc}, (V)	FF	Efficiency AM0, (%)
1605	109	0.99	0.74	14.6
1606	104	1.01	0.77	14.8
1607	106	0.94	0.77	13.5
1609	101	1.03	0.82	15.7
1610	102	1.03	0.81	15.5
1611	100	1.03	0.83	15.8
1612	105	0.98	0.77	14.4
1614	100	1.02	0.83	15.7

TABLE 5. CHARACTERISTICS OF GaAs SOLAR CELLS GROWN IN SUCCESSIVE LPE RUNS IN MAY 1978

Cell No.	I_{sc}, (mA)	V_{oc}, (V)	FF	Efficiency AM0, (%)
2063	102	1.00	0.70	13.2
2064	110	1.01	0.74	15.2
2065	113	0.99	0.72	14.9
2066	109	1.01	0.76	15.4
2067	110	1.01	0.74	15.2
2068	115	1.01	0.75	16.0
2069	118	1.00	0.75	16.4
2070	113	1.01	0.73	15.4

TABLE 6. CHARACTERISTICS OF RECENT GaAs SOLAR CELLS GROWN IN SUCCESSIVE LPE RUNS IN DECEMBER 1978

Cell No.	I_{sc}, (mA)	V_{oc}, (V)	FF	Efficiency AM0, (%)
2684	119	1.02	0.77	17.2
2685	115	1.01	0.78	16.8
2686	111	1.01	0.77	16.0
2687	114	1.01	0.76	16.2
2688	118	1.02	0.77	17.2
2689	119	1.02	0.78	17.4
2690	119.5	1.02	0.74	16.4
2691	113	1.01	0.76	15.9

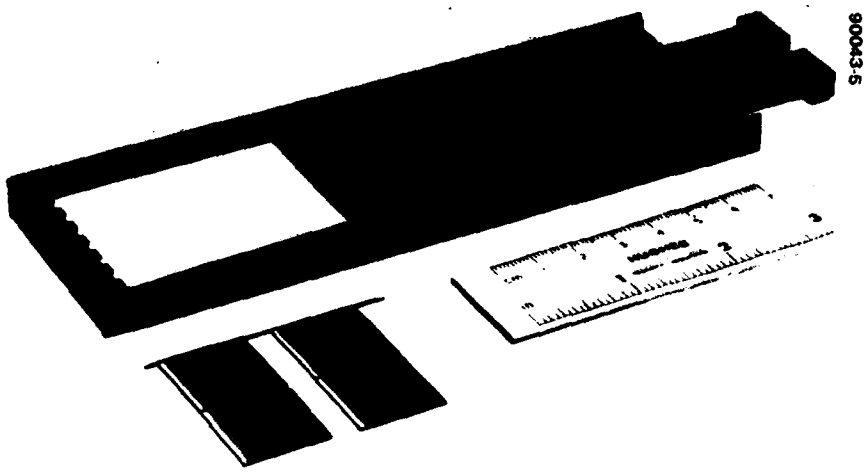

Figure 5. New substrate holder with large rectangular GaAs substrate.

These encouraging results resulted in an increase in the capacity of the substrate holder to four GaAs wafers. In addition, the size of each wafer was increased to 1 by 2 inches, allowing two 2 x 2 cm cells per wafer to be grown. A series of runs was made using this arrangement and the system parameters were tailored to ensure uniform conditions of growth for all four substrates. As a result of this effort it was demonstrated that the infinite solution LPE system can be modified to fabricate eight solar cell structures at a time. Consequently, two such systems are presently in operation, one for buffer layers and one for the (AlGa)As window layers. They have operated without any serious problems during the last few months. Typical cell characteristics are shown in Table 6.

In a latest modification, a single substrate holder has been enlarged to handle a 2 by 2 inch GaAs substrate that will yield 2 x 2 cm cells as shown in Figure 5. The system handles this large holder with no problems. Subsequent studies have also shown that the substrate capacity can be further increased to hold at least eight wafers at a time, thus making 32 separate 2 x 2 cm cells per run. The scale-up effectively leads to mass production capabilities by reducing the LPE growth time per substrate by a factor of 8 and enabling batch processing in subsequent fabrication steps. Such batch processing capability is essential for mass production of space qualified solar cells for satellite power applications.

Several interesting factors have emerged from experiments on larger systems. First, they are more controllable than are the smaller systems. This control largely results from the enhanced stability of the large solution and from the fact that the growth of a large number of layers is possible without appreciably affecting the concentration of the solution. It has been observed also that the large solutions are easier to bake out during the initial cleanup when the solutions are first made, and they maintain their purity for long periods without any subsequent cleaning. This advantage arises mainly from the lower surface to volume ratio of solution to the container and the substrate holder. Furthermore, lower growth temperatures can be maintained than in the case of smaller systems, and the temperature cycles can

be reduced in range since a larger amount of solute is available ex-solution for a small drop in temperature. Since the cooling rate can be reduced, there is also less probability of spurious nucleation occurring in the solution during the long-term buffer layer growth. The combined result of all these factors has resulted in more reproducible control over the characteristics of the epitaxial layers and, hence, of the device itself.

3.3 LPE Solution Parameter Control. The larger solution has made possible the study of the influence of various solution parameters more accurately. For example, the n type tin concentration for buffer layers is maintained $>1 \times 10^{17}$ cm^{-3} in order to yield a grown layer with $n = 1 \times 10^{17}$ cm^{-3}. It has been discovered that a solution maintains this concentration without any serious problem for a period of over 3 months, during which over 500 layers are grown from it. At this stage, the solution level falls, and it can be brought back up by the simple addition of Ga, GaAs, and Sn in the proportion that they are in the solution.

The (AlGa)As solution acts similarly especially if only thin window layers are grown. The Al concentration in the solution tends to drop progressively because of the segregation coefficient of Al which is approximately 50. However, the layer is so thin that several hundred layers can be grown from the large solution before being observably depleted of Al. Furthermore, ways of growing the layers well below saturation temperatures have been developed so that there is always an excess of (AlGa)As in the solution. Since the Al concentration of the solid is high, as it dissolves back it reestablishes the equlibrium value of the solution at the growth temperature. This process makes the window layers very reproducible in Al composition. Using this method in combination with the large solution, only the Be content needs to be replenished from time to time in order to produce several hundred layers.

The Be composition is controlled by adding about 5 mg of Be per 1000 gm of solution to provide $\sim 1 \times 10^{18}$ cm^{-3} carriers in the epitaxial layer. Adding higher Be amounts can adversely affect the layer quality. Apparently, this level is close to the maximum that is normally incorporated in the GaAs lattice. Additions above $\sim 2 \times 10^{18}$ cm^{-3} result in precipitates and higher dislocations which are harmful. In cell processing, they lead to channeling of the contacting metals causing leakage in devices. At a level of 1×10^{18} cm^{-3}, the layers are well behaved and do not develop surface degradation. As a result of these observations, the Be level has been kept close to this concentration in the epitaxial layer. For similar reasons of layer stability, the Al composition has been maintained at ~90 ±3 percent in the (AlGa)As window layer. These parameters yield cells with a V_{oc} of 1.0 volt and a short circuit current of 115 ±5 mA per 4 cm^2 cell.

In Table 7, the characteristics of four cells grown during a particular run using a single slide bar are presented. The cells numbered 1871 and 1872 came from the same substrate on one side of the slide bar while the

TABLE 7. EARLY GaAs CELLS GROWN IN A SINGLE RUN
(TWO SUBSTRATES)

	Cell No.	I_{sc} (mA)	V_{oc} (V)	FF	Efficiency AM0 (%)
*	1871	112	1.0	0.77	15.8
*	1872	109	1.0	0.77	15.5
*	1873	104	0.99	0.75	14.4
*	1874	104	0.98	0.74	14.0

*Both cells from single substrate.

other two were cleaved from a substrate positioned on the opposite side. The lower efficiency of the latter two was traced to the fact that the slide bar was not properly centered in the solution. This centering has since been corrected and cells from subsequent growths are more uniform in efficiency. Table 8 gives similar results of seven cells fabricated later in the HESP II program using a double slide bar. This device consists of two separate graphite substrate holders nearly identical to the one used for the cells in Table 7, except that both are suspended and submerged in the solutions simultaneously. Thus, the capacity of the run is effectively doubled. The cells of Table 8 indicate not only enhanced production capability but also higher efficiencies.

TABLE 8. LATER GaAs CELLS GROWN IN A SINGLE RUN
(FOUR SUBSTRATES)

	Cell No.	I_{sc}, (mA)	V_{oc}, (V)	FF	Efficiency AM0, (%)
*	2317	114	1.01	0.77	16.3
*	2318	112	1.01	0.76	15.8
*	2321	113	0.97	0.69	14.0
*	2319	109	1.01	0.76	15.4
*	2320	112	1.01	0.77	16.0
*	2322	113	1.01	0.74	15.6
*	2323	112	1.01	0.72	15.0

*Cells from single substrate.

3.4 Cell Fabrication. With the delivery of the GaAs substrate from a subcontractor, the cells are subsequently processed using the sequence derived through both theoretical and empirical considerations. During the first year of HESP II, this basic sequence has been developed and continually refined to enable the fabrication of 2 x 2 cm cells meeting the contract requirements. This perfected procedure forms the basis for the documentation presently underway which, in turn, is to be followed for the manufacture of qualification cells during the next several months. Deliverable cells follow the completion of this qualification testing.

During the development period of the program, much attention was devoted toward understanding and controlling the epitaxial growth temperature. This is the temperature at which growth is initiated on the substrate. Earlier in the program this parameter was set at 800°C. Attempts were made to slow down the layer formation in order to permit the reproducible growth of the critical ~0.5 μm window. However, when this was done, the junction depth was found to vary and sometimes exceeded the expected value (also 0.5 μm). Since the junction depth is critical in determining the hardness of the cell to radiation environment, a series of temperatures and growth times was tried in order to establish reliable guidelines for more controllable epitaxy. The final temperature selected was 750°C. At this temperature a layer approximately 0.4 ±0.1 μm could be formed in 4 minutes with a junction depth of 0.5 μm. Since this choice of parameters was suitable for fabrication of the HESP II baseline cell, the parameters remain as the operational values of the present epitaxial process.

Also studied was the influence of the n type buffer layer thickness on overall cell performance. Early results showed that a buffer layer thickness greater than ~7 μm is required to eliminate any noticeable substrate influence on cell efficiency. The n-layer thickness, therefore, is maintained at 9 ±2 μm.

Since the beginning of the contract, numerous other studies were conducted with respect to the ultimate quality of the expitaxial layers. In summary the following requirements were found to be significant:

1) An oxygen free ambient in the system

2) A Hall mobility of 80 $cm^2\ V^{-1}\ sec^{-1}$ for Be-doped (AlGa)As layers with a Be carrier concentration of $1 \times 10^{18}\ cm^{-3}$

3) Use of an etch and rinse procedure for substrates utilizing solvents and reagents of semiconductor purity

4) Use of deionized water with a resistivity of greater than 15 megohms

5) Maintainance of an Al concentration in the (AlGa)As layer of 90 ±3 percent.

3.5 Cell Production and Delivery. During the first year of the HESP II program, 70 cells have been delivered to AFAPL with power conversion efficiency in excess of 15 percent AM0. This meets all the delivery requirements during this period.

One of the important studies in connection with the program was to establish a rate of improvement in yield as a function of time. During the early part of the program, several parameters had to be optimized and the contracts were still causing some problems. As these were ironed out and the process was streamlined, the yield of cells became more predictable. In Table 9 the distribution of cells produced during 2 month periods is shown

TABLE 9. GaAs SOLAR CELL YIELD VERSUS EFFICIENCY, SEPTEMBER 1977 TO DECEMBER 1978

Time	AM0 efficiency, (%)	Yield/start, (%)
September to October 1977	⩾15	22
	⩾16	4
	⩾17	0
May to June 1978	⩾15	45
	⩾16	21
	⩾17	5
November to December 1978	⩾15	61
	⩾16	47
	⩾17	18

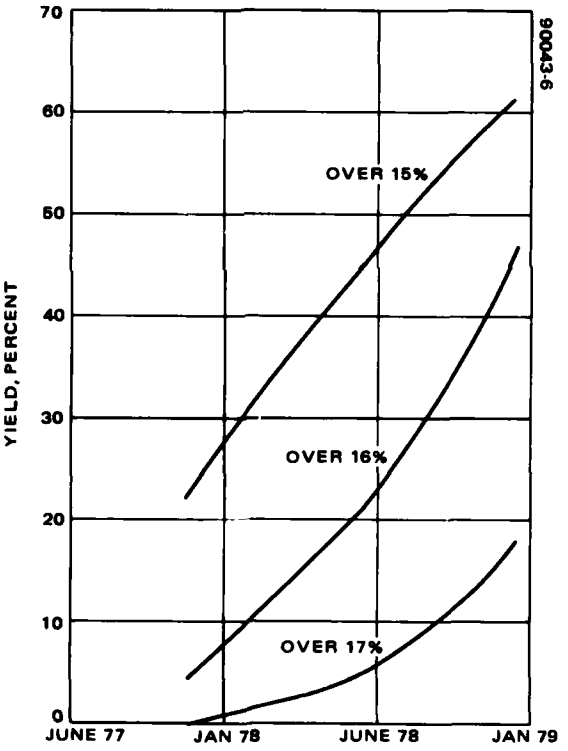

Figure 6. Cell yield for September 1977 through December 1978.

at the beginning, the middle, and the end of the first year of HESP II. The numbers in the table and the distribution curves shown in Figure 6 show the steady improvement both in the quality and the quantity of cells as a function of time. During the last 2 months, the yield of cells with efficiency higher than 16 percent approached 50 percent of all the cells processed.

4. GaAs CELL METALLIZATION

4.1 General Background. Aside from the epitaxial growth, the major emphasis on cell fabrication falls on the contacting procedures used. A non-trivial task is forming reliable ohmic contacts that can adhere to (AlGa)As.

Contacts to semiconductors are empirical at best. One or more metals are applied to the semiconductor surface with a dopant and a fluxing transition metal such as Ni, Cr, Pd, or Ti. For the n GaAs such contacting systems are available. AuGeNi and AgSn are good examples, the former for a 450°C contact and the latter for one with somewhat higher temperature capability (600°C). AuGeNi was chosen as the first candidate since it is compatible with the AuZn system for the p type material; the latter has been most often used for p type GaAs contacts.

Having chosen the alloys, the next question was the best technique of metallization for optimum results. The advantages and disadvantages of various techniques of contact metallization are illustrated in Table 10. The two most commonly used methods are evaporation (either thermal or E beam) and sputtering (RF or dc using ion beams). The evaporation method implies high temperatures, but since the metals are so different in vapor pressures (Au and Zn), it was believed sputtering would have some advantages in control. Therefore, sputtering was selected as the main approach.

TABLE 10. CONTACT METALLIZATION TECHNIQUES

Method	Advantages	Disadvantages
Evaporation		
Thermal	Simple, standard technique	General heating due to evaporation temperature
E beam	Sequential deposition of metals	High vapor pressure of zinc
Sputtering		
Ion beam	Low temperature, especially for Zn	Oxide problem: function of oxygen background
RF	Mechanical adhesion due to bombardment	Need to control oxide on (AlGa)As
		Control of composition of metal empirical

Another consideration was the choice of contact grid patterns on the p side. The typical grid pattern used is a 24 finger pattern. It is a good compromise because of minimum shadowing (~5 to 8 percent) and good

collection efficiency. This pattern could be produced using either photolithography or mechanical masks. HRL has been developing both techniques concurrently for use in a variety of applications. For a cell compatible with concentrated illumination, the photolithographic technique is especially useful since it provides the high resolution necessary for the closely spaced contact pattern required to minimize series resistance in high current operation. However, for high efficiency cells at low concentrations a mechanical mask approach offers a simpler technique that is compatible with silicon solar cell practice, which is a significant factor in establishing a rapid transition to production for GaAs solar cells. Thus, the mechanical mask approach was chosen utilizing the standard 24 finger mask used for silicon 2 x 2 cm space cells.

The feasibility of ultrasonic seam welding tabs onto the contacts deposited is yet another important aspect of the HESP II contract. Areas of concern include the electrical characteristics of cells after the welding operation and mechanical strength of the resulting bonds as well.

4.2 Contact Metallization Techniques. Figure 7 shows the complete GaAs solar cell fabrication process in which the ohmic contacts are given detailed attention.

The best results for the AuZn contacts to the p type (AlGa)As cell surface have been achieved using a sputtering technique. However, the AuGeNi n type contacts have been applied using simple thermal evaporation. Both sets of contacts are now under good control and will be applied by the developed techniques for the qualification cells.

The AuGeNi n type contacts are particularly easy to apply. The proportions involved are 12 percent Ge, 1.5 percent Ni, and 86.5 percent Au by weight. A coat of about 2000 Å is used, and this is covered over by a 5 μm Ag overlay.

The AuZn contact is composed of about 15 percent Zn and 85 percent Au by weight. The Au and Zn were initially sputtered onto the p surface from a composite target. However, since the new sputtering system acquired recently has multiple targets, the technique of sputtering from two targets of Au and Zn separately has been perfected. This method provides considerably greater flexibility and reproducibility. The AuZn layer is also approximately 2000 Å thick and is covered with 5 μm of Ag.

After both the n and p type contacts are deposited, they are annealed at a temperature of 480°C in a furnace specially set up for this purpose. It was discovered early in the program that it is extremely important to eliminate all traces of oxygen from the annealing furnace in order to avoid deterioration of the (AlGa)As surface by oxidation and to prevent mechanical weakening of the contacts themselves. This deterioration effect was significant, especially on the bar type contacts, since any weakening of these leads to an increase in the series resistance and sometimes increased leakage which causes lower power conversion efficiency. Since the new annealing furnace with a Pd diffused hydrogen ambient has been onstream, the contact adhesion and ohmicity

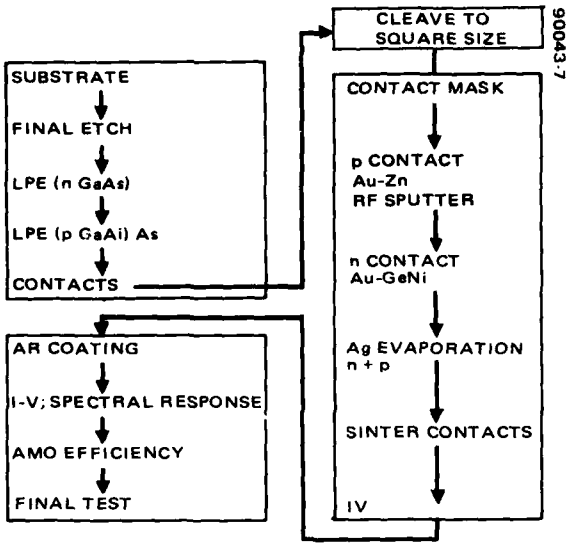

Figure 7. GaAs solar cell fabrication process.

have been both reproducibly good, and the cell fabrication yields have steadily improved.

In addition to developing the AuZn and AuGeNi contacts, work has been done on AgZn and AgSn contacts. The silver based contacts can lead to improvement in two significant areas. First, they are capable of higher temperature operation (600 versus 400°C). Secondly, they would eliminate Au, which is costly. In addition to these direct benefits, there is another advantage in that the whole contact deposition can be handled in a sputtering system with three targets: Ag, Sn and Zn, thus reducing manufacturing process steps. The preliminary results obtained have been very encouraging. As shown in Table 11, the cells have reasonably good characteristics. However, the composition of the contacting alloys and the annealing cycles have to be defined with much more precision to ensure reproducibility. Also, the mechanical integrity of the contacts for welding and under various ambient conditions has to be established.

TABLE 11. GaAs SOLAR CELL CHARACTERISTICS
(AgZn Contacts on P Side)

Cell No.	V_{oc}	I_{sc}, (mA)	FF, (%)	Efficiency AM0 (%)*
2393	1.01	119	78	17.3
2395	1.02	119	77	17.2
2451	0.99	111	77	15.6
2517	1.01	110	75	15.4

*Efficiency after AR coating.

In summary, the AuZn p type contact has been developed for the HESP II cells in combination with the AuGeNi system for the n type. These contacts are both overlaid with 5.0 μm of Ag and are then annealed at 480°C. In addition, sufficient environmental tests have been performed to prove their low resistance and mechanical integrity, and their applicability to welded interconnection has been demonstrated.

4.3 Ultrasonic Seam Welding. The HESP II contract explicitly requires that interconnects be welded. As a result, GaAs cells fabricated at HRL were sent to the Space and Communications Group for attaching permanent interconnects to both the top and bottom metallized contacts using an ultrasonic seam welder.

The facility in producing reliable welds is not consistent but instead depends heavily on the particular conditions of the system to be welded. For example, the ability to weld thick Mo to polished sapphire will differ considerably from bonding Au leaf to severely abraded graphite. Thus, weldability is a function of, among other things, substrate material, component surface conditions, contact/tab composition, and cross-sectional geometry, in addition to sensitive equipment controls and operation techniques.

4.3.1 Interconnect Composition and Size. Interconnects were constructed from 99.99 percent Ag foil 1.0 mil thick. Units prepared for welding were made up of six tabs, each originally connected as shown in Figure 8. Welds were made by placing the fingers over the solar cell contact and running the weld wheel from A to A'. The foil was then cut along the dashed lines and individually separated following the welding operation. Thus, attached to the completed cell were 12 independent tabs, each approximately 1.1×6.5 mm^2 in area.

4.3.2 Welding Apparatus. A simplified block schematic of the ultrasonic seam welder and supporting equipment is shown in Figure 9 (the horizontal plane is the surface of the figure; the vertical direction is into the diagram). Here the welding tool is a 0.71 inch diameter wheel machined from drill rod and attached to a 6 inch long tapered horn rigidly connected to a magnetostrictive (ferromagnetic) transducer. This entire unit is spring mounted to a block in such a way that the spring tension and thereby the contact force F_c of the wheel against the device can be increased or decreased in the vertical direction by means of set screws (not shown). The block, in turn, can be motor driven along a track in the horizontal plane at various speeds.

The transducer is controlled by a power source equipped with both amplitude and tuning adjustments. Relative scales associated with each ensures reproducibility of settings. Tuning is further facilitated using an oscilloscope displaying a Lissajour pattern resulting from simultaneously monitoring the current and voltage through the transducer.

The vacuum stage supports both the solar cell and tabs during welding while the calibration stage is used to determine the contact force F_c of the wheel by means of a simple switch circuit.

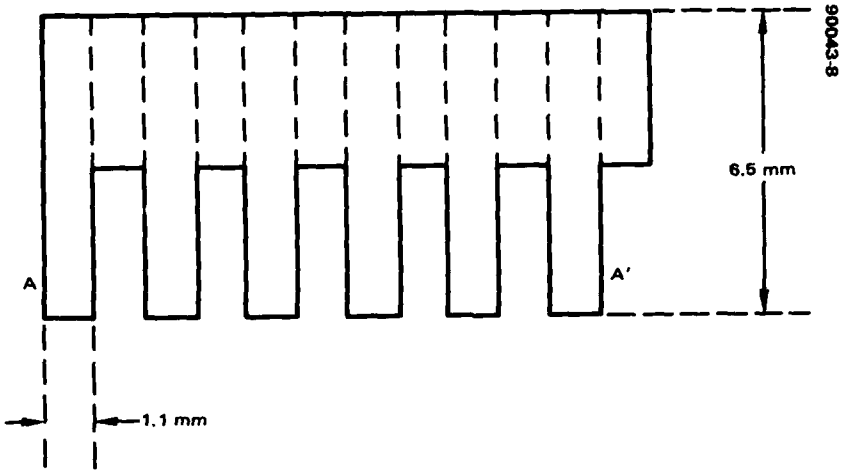

Figure 8. Silver foil pattern with six tabs.

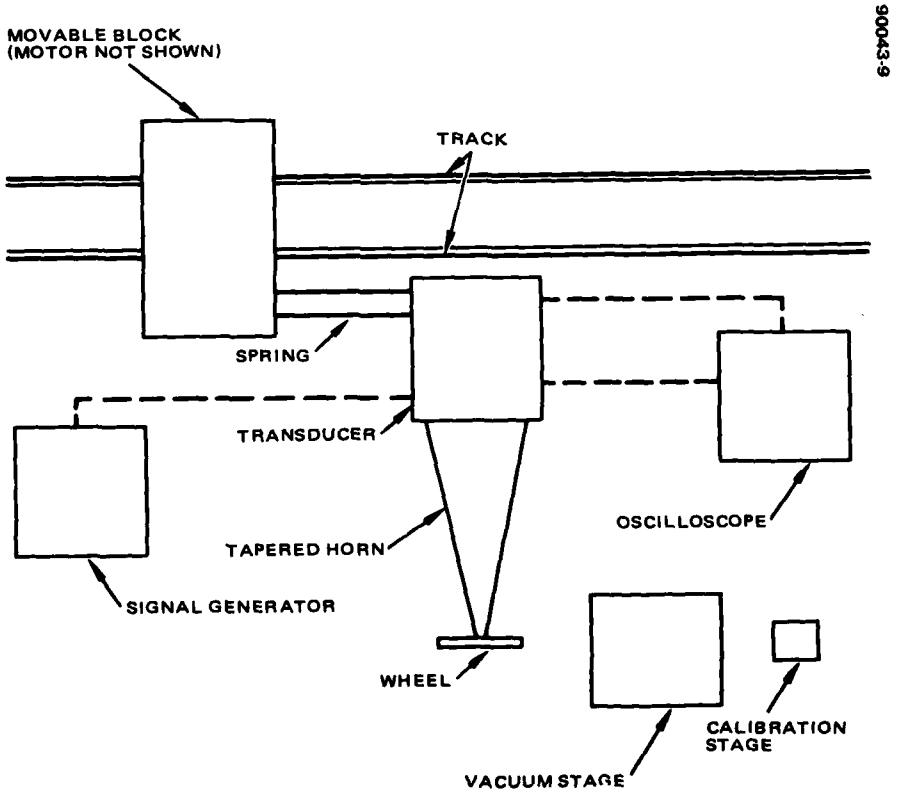

Figure 9. Top view schematic of ultrasonic seam welder and supporting equipment.

Producing reliable bonds entails a trial and error procedure to determine the optimum values of the following four key parameters:

1) F_c, contact force — This force is that which the weld wheel exerts upon the tab/cell combination during welding. It is capable of being adjusted through a range from zero to well over 450 grams.

2) P, relative power output of the source — This adjustment modifies the amplitude of the electromagnetic wave transformed by the transducer into mechanical oscillations eventually delivered to the weld area.

3) T, tuning of the source — Tuning alters slightly the frequency of the electrical signal and thereby the mechanical energy introduced to the weld. By proper tuning, the energy delivered to the weld wheel can be maximized by matching the resonant frequency of the horn/wheel assembly.

4) V, velocity of the wheel — The speed at which the weld wheel travels over the weld area determines in part the total amount of energy imparted into the bond which, in turn, affects the quality of the bond.

Extensive preliminary testing was done in order to determine the relationship of each of these weld parameters to the resulting bond strength. Figures 10 through 13 exhibit the results. In summary it can be seen that each of the parameters affects bond quality dramatically. Yet all the parameters are interdependent. This is best illustrated in Figure 10 in which extremely strong bonds (>600 gms) can be obtained only when power peaks at about 5 (arbitrary units) and F_c is maintained at 400 grams. For a broader power range, F_c must be decreased to 250 grams. True, the resulting bond strength drops to approximately 450 grams, but an advantage is greater ease in the welding operation.

More detailed results of the welding study are reserved for Section 6, in which mechanical, electrical, and scanning electron microscopy (SEM) studies are presented.

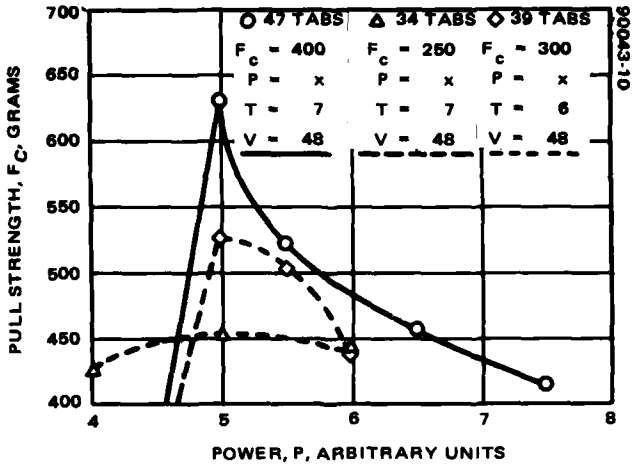

Figure 10. Pull strength as function of power,P.

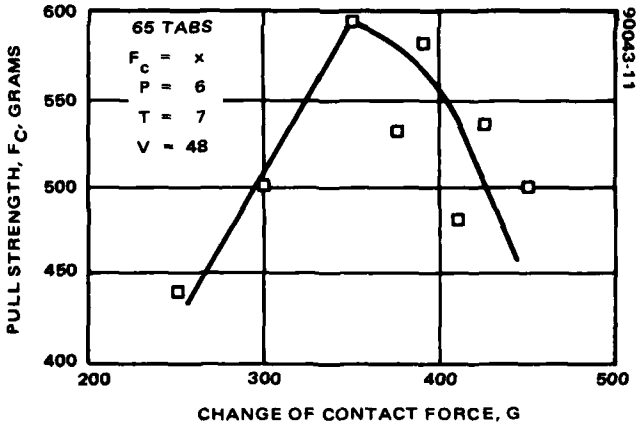

Figure 11. Pull strength as function of contact force, F_c.

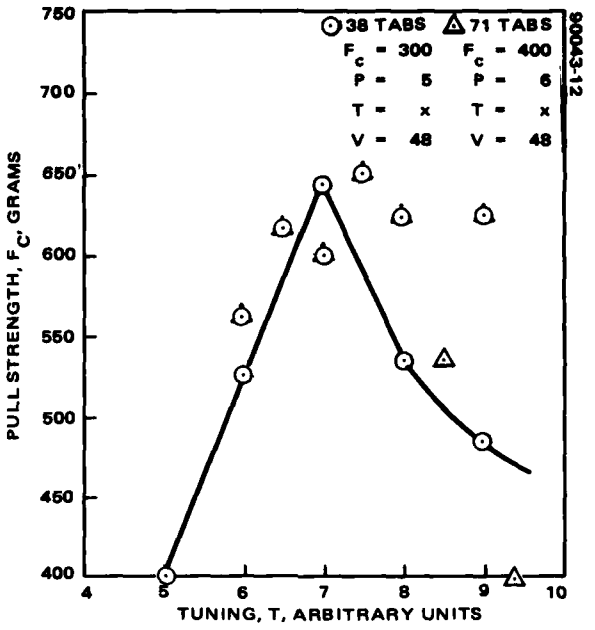

Figure 12. Pull strength as function of tuning, T.

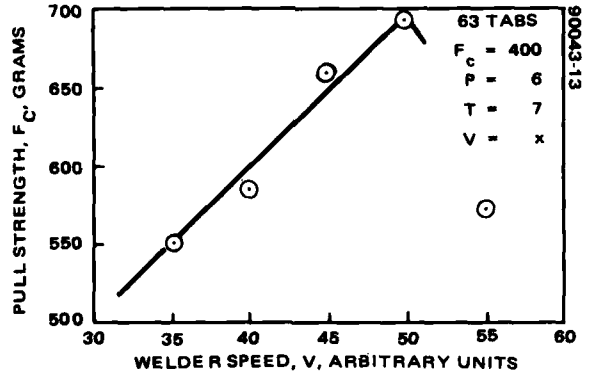

Figure 13. Pull strength as function of welder velocity, V.

5. GaAs SUBSTRATE

5.1 Introduction. The actual mechanism for energy conversion in GaAs solar cells, takes place in the uppermost surface. With the present process this critical GaAs layer is grown by liquid phase epitaxy (LPE) upon a relatively inexpensive GaAs substrate, which provides both electrical connection and mechanical support. An important effort with respect to this contract was the development of speedy, cost-effective methods to manufacture large area, rectangular GaAs substrates.

Thus, one of the goals of the contract was to study the horizontal Bridgman growth technique in producing GaAs single crystals with large area rectangular cross sections. A resulting slice with a 2.0 by 1.0 inch surface area would increase the usable material and thus reduce the cost. Wafers with cross sections as large as 2.0 by 2.0 inches would be even more effective.

Another area of concern was the reduction of the large GaAs crystals into appropriate substrate wafers. This involves two major processes: sawing and polishing. Various methods of sawing and polishing were examined in an attempt to produce GaAs wafers in less time, with better mechanical characteristics and less breakage – in short, more economically.

Finally, attention was focused on processing thinner GaAs substrates. After attempts at making 12 mil wafers, the feasibility of 8 mil wafers was to be studied. Such a reduction in thickness would result in lighter GaAs solar cells. In addition, if the 8 mil substrates could be sliced thinner from the beginning, more GaAs cells would result from the same crystal.

In the following sections a description of the horizontal Bridgman technique of growing single crystal GaAs is given. This is followed by assessments of the large area substrates so produced, the various methods of subsequent sawing and polishing wafers, and the feasibility of thin GaAs slices.

5.2 Horizontal Bridgman Crystal Growth. The technique of growing crystals by the horizontal Bridgman technique usually involves a two zone furnace to produce a temperature gradient which is translated horizontally to cool a melt composed of the material which is being grown into a single crystal. However, for GaAs crystals a third furnace is used to control the arsenic temperature during reaction. A schematic of the equipment required

is displayed in Figure 14. The sealed quartz growth ampoule shown contains a boat loaded with a single crystal seed, GaAs melt, and quantities of elemental Te and As. The ampoule, in turn, is enclosed within the three zone furnace, which can be translated.

The first step in actual GaAs growth involves the complete cleaning of all materials that would come in contact with the gallium and arsenic during growth. Materials such as the boat (quartz, graphite, or vitreous carbon), the quartz growth ampoule, and the support liners are etched using a 1:1 mixture of nitric and hydrochloric acid. Afterwards these materials are thoroughly washed in deionized water.

The gallium is then placed in the boat with a seed crystal in the front portion of the vessel. The support liners are placed on the sides and under the boat (if a quartz boat is used). A small amount of tellurium dopant is placed on the growth ampoule in front of the boat. A stoichiometric amount of arsenic is then placed in the other end of the growth ampoule. The quartz growth end and arsenic end are then sealed with a quartz rod to form the growth ampoule. The ampoule is subsequently evacuated and sealed at the front of the growth end by collapsing and removing the quartz vacuum tube.

After this, the ampoule is placed in the furnace, and the gallium and arsenic are reacted by heating the gallium to the melting point of GaAs (1247°C) while the arsenic temperature is held at 600°C. At this temperature the arsenic sublimes and reacts with the gallium, forming the GaAs melt. The GaAs melt is then allowed to soak for 24 hours to aid single crystal growth. After adjusting the melt and growth zone temperature to a level where the molten GaAs just melts into the seed, the furnace is caused to travel, thus slowly cooling the material below the melting point of GaAs. The rate of travel of the furnace is about 0.5 inch per hour.

After the crystal is grown, it is taken from the furnace, and slices from the front and back of the crystal are removed to obtain EPD and Hall data. After these measurements are made the crystal is cut to the desired size and mounted in preparation for wafering on either the ID saw or multiblade saw.

5.3 Large Area GaAs Substrates — Assessment. To obtain rectangular GaAs crystals, a boat material had to be found which could physically hold the weight of the melt and at the same time be compatible with good crystal growth. This endeavor eventually led to the evaluation of fused quartz, graphite and vitreous carbon boats. In addition, to support the bottom and sides of the rectangular quartz boats, liners made of silicon carbide, boron nitride, and fused quartz were assessed. The placement of such liners about the boat is illustrated in Figure 15. Using these materials in various combinations, their effects on crystal perfection and crystal uniformity were studied on resulting GaAs ingots with a minimum cross section of 1.0 by 2.0 inches and a preferred cross section of 2.0 by 2.0 inches.

A summary of all growth runs and results is listed in Table 12. The resulting assessment of boat and liner materials and of the feasibility of large area substrate growth is given below the table.

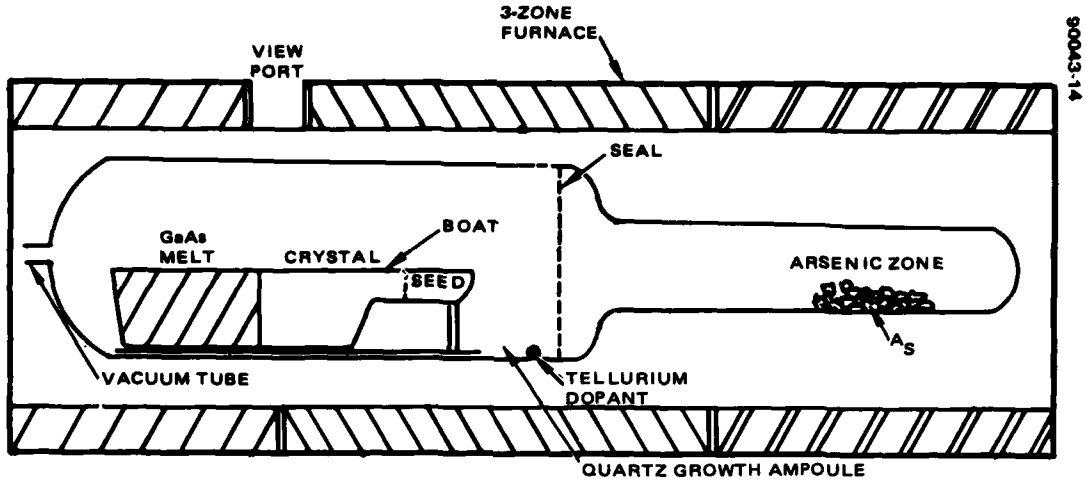

Figure 14. Horizontal Bridgman Growth.

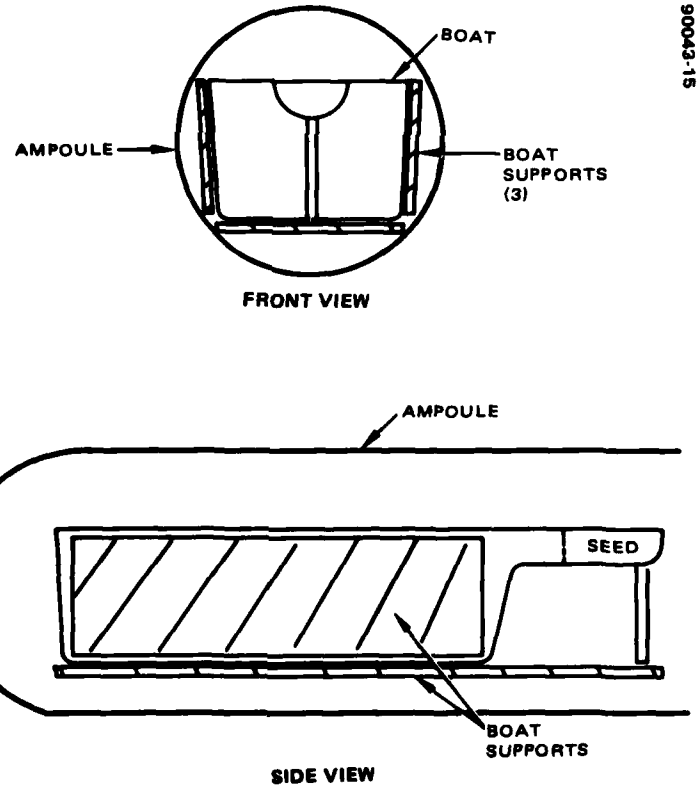

Figure 15. Boat supports.

TABLE 12. LARGE AREA GaAs SUBSTRATES – ASSESSMENT GROWTH RUNS

Runs made	Boat size, (in.)	Material	Liners	Orientation	Results
2	1.0 x 2.0	Quartz	Silicon carbide	(100) 110 up	Poly – oxides
3	1.0 x 2.0	Quartz	Quartz	(100) 110 up	Single
5	2.0 x 2.0	Quartz	Quartz	(100) 110 up	Poly – steep thermal gradients
6	1.0 x 2.0	Quartz	Boron nitride (BN)	(100) 110 up	Poly – boat wet
8	1.0 x 2.0	Graphite	None	(100) 110 up	Poly – oxides, boat wet
9	1.0 x 2.0	Quartz	BN	(110) 100 up	Single
11	1.0 x 2.0	Quartz	BN	(110) 100 up	Single
12	2.0 x 2.0	Quartz	BN	(110) 100 up	Poly – steep thermal gradients
15	1.0 x 2.0	Quartz	BN	(110) 100 up	Single
16	1.0 x 2.0	Quartz	None	(110) 100 up	Single – boat sagged
19	1.0 x 2.0	Quartz	BN and Quartz	(110) 100 up	Single
20	1.0 x 2.0	Quartz	BN	(110) 100 up	Poly – oxides
22	1.0 x 2.0	Vitreous carbon	None	(110) 100 up	Poly – boat wet
23	1.0 x 2.0	Quartz	BN	(110) 100 up	Single
24	2.75 x 1.0	Quartz	BN	(110) 100 up	Poly
25	2.0 x 2.0	Quartz	BN	(100) 110 up	Poly – steep thermal gradients
26	2.0 x 2.0	Quartz	BN	(100) 100 up	Poly – steep thermal gradients
27	2.75 x 1.0	Quartz	BN	(110) 100 up	Single
28	1.0 x 2.0	Quartz	BN	(110) 100 up	Poly – melted seed
29	1.0 x 2.0	Quartz	BN	(110) 100 up	Poly – oxides
30	1.0 x 2.0	Quartz	BN	(110) 100 up	Single
31	1.0 x 2.0	Quartz	BN	(110) 100 up	Single
32	1.75 x 1.5	Quartz	BN	(110)	Single
33	1.0 x 2.0	Quartz	BN	(110) 100 up	Poly – oxides
34	1.0 x 2.0	Quartz	BN	(110)	Single
35	1.75 x 1.5	Quartz	BN	(110)	Single

5.3.1 Quartz Boats and Liners. Very early growth attempts in quartz resulted in considerable difficulty attributed to boat wetting. With changes in cleaning techniques, however, such wetting has been significantly reduced. Especially good single crystals were obtained in 1.0 by 2.0 inch quartz boats using boron nitride liners (runs 9, 11, 15, 23, 30, 31, and 34 of Table 12).

For support, silicon carbide liners were used in run 2. However, this resulted in the formation of a crystalline residue on the inside walls of the ampoule. In addition, a scum accumulated on the surface of the melt. Silicon carbide, therefore, is not considered to be a good liner material.

Quartz plates and rods were also used as liners (runs 3, 5, and 19), and subsequent growths for the most part proved to be single crystals. However, due to the high growth temperature needed for GaAs, they became distorted and tended to fuse to the quartz boat and ampoule.

Ingots 5, 12, 25, and 26 were grown in 2.0 by 2.0 inch quartz boats, but the material proved to be polycrystalline. This was probably due to the thermal gradients throughout the 2.0 inch depth of the boat. On the other hand, single crystals resulted in runs 32 and 35 which were grown in boats 1.75 inches wide and only 1.5 inches deep.

Therefore, 2.0 by 1.0 inch and 1.75 by 1.5 inch quartz boats with boron nitride support liners seem to be the most feasible way of growing single rectangular GaAs crystals. By cutting these selectively, substrate wafers with four surface areas can be regularly produced: 2.0 by 1.0 inches, 2.0 by 2.0 inches, 2.25 by 1.5 inches, and 1.75 by 1.5 inches.

The 2.0 by 1.0 inch and 1.75 by 1.5 inch boats come from standard size rectangular quartz stock. For boats with cross sections other than these dimensions, specially drawn quartz is required.

5.3.2 Graphite Boats. Run 8 was done in a 2.0 by 1.0 inch high purity graphite boat. A single crystal could not be grown because of a dross which floated upon the surface of the melt. Upon removal of the crystal from the furnace:

1) The top of the crystal was coated with many particles. These bubble like deposits were scattered over the entire upper surface area. The particles probably came from the carbon boat. Historically, growth in carbon boats has not been successful, mainly because of these particles.

2) Difficulty was experienced in removing the crystal from the boat. This boat wetting effect usually occurs in quartz boats (primarily due to moisture in the quartz itself) and in the past has not been a problem with carbon boats.

Because of these effects, graphite is not considered to be a suitable boat material.

5.3.3 Vitreous Carbon Boats. Crystal 22 was grown in a 1.0 by 2.0 inch vitreous carbon boat made at Tylan Corporation by placing a high purity vitreous coating over a carbon boat. Single growth was attempted four separate times but could not be attained. There were no bubble-like particles on the surface of the crystal as was the case with the carbon boat. Apparently the vitreous (glassy) coating helped prevent carbon from leaving the boat and entering the melt. However, the crystal adhered severely to the boat, again indicating wetting.

5.3.4 Summary. As a result of this study, carbon and vitreous carbon boats were determined to be unsuitable for GaAs crystal growth. Quartz boats were found to be the best material, after proper cleaning to minimize boat wetting. However, at and above the melting point of gallium arsenide (1247°C), the quartz will soften and begin to sag under the weight of the growing crystal. To properly support growth, high temperature resistant liners are necessary. Boron nitride liners were found to be the most suitable liners.

Using the quartz and boron nitride combination, GaAs ingots can be grown that are capable of being processed into large area rectangular substrates having surfaces of 2.0 by 1.0 inches, 2.0 by 2.0 inches, 2.25 by 1.5 inches, and 1.75 by 1.5 inches.

5.4 Sawing and Polishing Process – Assessment. After the GaAs crystal is grown, it must be cut into wafers using either of two techniques – the inner diameter (ID) saw or the multiblade saw. A description of each follows.

5.4.1 Sawing Methods. The ID saw incorporates special orientation fixtures designed for unusual cutting angles which are necessary with GaAs crystals. The saw blade itself remains stationary while the mounted ingot moves through the blade. Blade flutter, the prime cause of gross subsurface damage in semiconductor wafers, is held to a minimum, and extremely close mechanical tolerance is possible. Saw marks and surface imperfections are not discernible if the machine is properly maintained.

The multiblade saw employs up to 240 thin oscillating steel bands. An abrasive slurry does the actual cutting, usually resulting in an extremely smooth surface ready for lapping and polishing. It was felt that with the use of such a machine with blades that produce a kerf loss of 0.007 inches, the waste due to cutting and polishing could be reduced to about 54 percent of the present figure. Other savings in breakage and labor might also be realized.

5.4.2 Post-Saw Processing. After the crystal is sliced, the wafers are ultrasonically cleaned in sulfuric acid and then mounted on a flat stainless steel plate using a high purity microcrystalline wax. Five micron platelet alumina grit is used for precision lapping of the wafers to the desired thickness. This process is followed by polishing.

Mechanical polishing produces extremely flat wafers. However, there is always attendant subsurface damage. Chemical polishing, on the other hand, produces wafers that are relatively free of subsurface damage but are not optically flat. Chemomechanical polishing is the happy compromise. A chlorine bleaching solution acts as a mild chemical etchant while a polishing pad gently planes the surface resulting in a flat surface with virtually no damage.

After polishing, the wafers are cleaned by boiling them in trichloroethylene. The wafers are then inspected for correct thickness and any physical damage before being accepted for LPE growth.

5.4.3 Evaluation of Saw Methods. The initial tests using the multiblade saw were very positive; results are shown in Table 13. Crystal 11 was cut using 0.004 inch blades and 0.021 inch spacers. Crystals 15 and 16 were cut with 0.004 inch blades and 0.023 inch spacers. Each of these crystals was sandwiched between 2 glass plates in a gypsum cement mold. The objective in using the plates was to reduce wandering and to dress the blades as they cut through the GaAs crystal. There were very few broken slices as a result of the cutting operation. The multiblade saw provides for a more uniform wafer thickness with less kerf loss than the ID saw. Most of the wafers sliced on the multiblade saw varied ±0.0005 inches per slice as compared with a ±0.002 inch variance on the ID saw. Kerf loss on the multiblade saw was also substantially reduced: from 0.013 inches on the ID saw (runs 23, 30, 31, 32, 34) down to about 0.007 inches (runs 11, 15, 16) on the multiblade saw.

On the other hand, the setup time for orientation, mold fabrication, and alignment of the crystal in the multiblade saw is 3 or 4 hours longer than the setup time for the ID saw. Maximum cutting time of 2.0 by 2.0 inch wafers on the multiblade saw, based on a 16 hour run to cut an entire crystal (with setup time), amounts to approximately 12 slices per hour. This compares with 20 slices per hour on the ID saw. Also, after using the multiblade saw blade damage was eventually detected that penetrated the entire thickness of many of the wafers. This damage was probably due to vibrations in the saw during direction changes of the blade head which forced the crystal to oscillate vertically. To correct the problem, the saw would have to be run at about half its current speed, and this would be too slow to be of practical use.

5.4.4 Summary. Because of damage induced by the multiblade saw, it cannot be considered an acceptable method of slicing GaAs crystals, and as a result its use was terminated. Crystals sliced after run 30 (Table 13) were done on the ID saw. The wafers coming off this saw had a flatness of 0.021 ±0.002 inches. This was greater than the 0.0005 inch variance of the multiblade saw. This variance, however, can be reduced during the lapping and polishing operation. The advantages in using the ID saw, as compared with the multiblade saw, is that it takes less time to slice ingots and there is less subsurface damage.

After slicing and lapping, a polishing process is required to finish the wafers. Simple mechanical polishing was found to induce subsurface damage in the GaAs, while the simple chemical technique yielded substrates not sufficiently flat. A chemomechanical polishing process was therefore developed to minimize the disadvantages of both of these methods.

5.5 Thin GaAs Substrates – Assessment. The last column of Table 13 indicates that both 12 and 8 mil substrates have been processed. However, yields and causes of breakage differ for the two thicknesses. An assessment of both groups follows immediately.

5.5.1 Evaluation of 12 Mil Wafers. Wafers that were sliced on either the ID or multiblade saw were approximately 0.021 inches as they came directly off the saw.

TABLE 13. SAW AND YIELD DATA

Run No.	Saw used	Wafers cut	Saw damage	Average kerf loss, (in.)	Lapping and polishing damage	Cleaning and mounting damage	Final inspection (cracks, inclusions, handling)	Good (shipped to Hughes)	Mils, (in.)
11	Multiblade	23	1	0.0005	3	3	–	16	0.012
15	Multiblade	26	1	0.0007	1	2	2	20	0.012
16	Multiblade	26	2	0.0008	?	3	1	18	0.012
23	ID saw	24	3	0.012	–	–	4	17	0.012
30	ID saw	29	–	0.014	–	–	4	25	0.012
		128						96 (75%)	
31	ID saw	24	2	0.014	–	3	8	11	0.008
32	ID saw	25	2	0.013	1	2	17	3	0.008
34	ID saw	24	2	0.014	–	6	4	12	0.008
		73					29 (45%)	26 (35%)	

The damaged wafers that were lapped and polished down to 0.012 inches (runs 11, 15, 16, 23, and 30) had various reasons for being rejected. Most of the losses were the result of breakage during sawing, damage during lapping and polishing, breakage during cleaning and mounting, and rejects due to cracks or inclusions discovered during final inspection.

Out of the 121 wafers that were lapped and polished to 12 mils, 96 (75 percent) were acceptable for subsequent LPE growth. Wafers with cracks and inclusions caused most of the rejections (11). Eight wafers were damaged during cleaning and mounting. Seven wafers were broken on the saw, and six wafers were damaged during lapping and polishing.

5.5.2 Evaluation of 8 Mil Wafers. The wafers that were lapped and polished down to 0.008 inch (runs 31, 32, and 34) had a higher rate of wafer breakage during cleaning and handling operations.

Out of the 67 wafers so processed only 26 (38 percent) were good. More than half of the damage was a result of breakage during the handling of these very thin sections in final inspection. Breakage of 11 others occurred during cleaning and polishing. In addition, six were damaged by the ID saw, and only one was damaged during lapping and polishing. This higher breakage rate can be reduced with modifications in the techniques used for the cleaning and handling.

6. TEST RESULTS

6.1 Temperature Cycling Test. The temperature cycling test of this subsection and the temperature-humidity test described below were performed under separate contract (AFAPL contract F33615-76-C-2121). In both tests, however, the state of the art GaAs solar cells examined were identical to those fabricated at the beginning stage of the HESP II contract. The purpose was to determine the effects of extreme environmental changes upon contract metallization in particular and power degradation in general. Because of this, the results of these studies are most relevant to the present contract and, accordingly, are reported. Significantly, more extensive temperature cycling and temperature humidity testing is scheduled with respect to the most recent HESP II GaAs solar cells as part of the qualification test plan.

In the temperature cycling test, cells were cycled 100 times between extremes of -195° and +100°C during which the minimum rate of change was 100°C/minute. In all, six individual cells were tested; for each, the current-voltage characteristics were taken both before and after cycling. The test description and the results are summarized in Tables 14 and 15. The

TABLE 14. TEMPERATURE CYCLE TEST DESCRIPTION

Parameter	Values
No. of cells	6
No. of cycles	100
Range	-195° to +100°C
Rate	100°C/min
Test	Before and after I-V characteristics

TABLE 15. TEMPERATURE CYCLE TEST RESULTS

Cell	V_{oc}, (mV) B	V_{oc}, (mV) A	ΔV_{oc}, (%)	$P_{V=775}$, (mW) B	P_{V-775}, (mW) A	$\Delta P_{V=775}$ (%)	I_{sc}, (mA) B	I_{sc}, (mA) A	ΔI_{sc}, (%)
1033	969.6	969.6	0	78.28	78.28	0	111.5	110.8	-0.63
1093	977.6	977.6	0	76.80	76.80	0	108.4	108.4	0
1086	953.6	955.2	+0.17	76.26	74.79	-1.93	110.4	110.9	+0.45
950	996.8	995.2	-0.16	78.28	78.28	0	110.8	111.4	+0.54
1013	966.4	966.4	0	80.06	74.09	-7.46	114.2	111.5	-2.36
1095	974.4	972.8	-0.16	78.51	77.50	-1.29	101.0	108.4	-0.55
Average 1	973.1	972.8	-0.03	78.03	76.62	-1.81	110.7	110.2	-0.45

Note: B = Before, A = After.

resulting average degradation of V_{oc} proved to be only -0.03 percent for which individual changes ranged from -0.16 percent to +0.17 percent. The average ΔI_{sc} was -0.45 percent but varied in separate instances from -2.36 percent to +0.54 percent. Finally, the average change of power (arbitrarily chosen at the point where the voltage equaled 0.775 volts) fell to -1.81 percent. Here, in an exceptional case, the maximum individual degradation was -7.46 percent. Other than this value, power changes ranged from -1.93 percent to 0.0 percent. Significantly, these values are accurate only to within ±1.0 percent.

Temperature tests to GaAs cells were not limited to the above. Additional experiments designed to examine the effect of environment on the contact metallization are reported in subsection 6.3.

6.2 Temperature-Humidity Test. The temperature-humidity test was performed on six GaAs cells. Exposure was to an atmosphere of at least 45°C and a relative humidity of 90 percent minimum for a period of 10 days. The test description and the results are summarized in Tables 16 and 17.

TABLE 16. TEMPERATURE-HUMIDITY TEST DESCRIPTION

Parameter	Figures
No. of cells	6
Temperature (min)	45°C
Relative himidity	90%
Duration	10 days
Test	Before and after I-V characteristics

TABLE 17. TEMPERATURE HUMIDITY TEST RESULTS

Cell	V_{oc}, (mV) B	V_{oc}, (mV) A	ΔV_{oc}, (%)	$P_{V=775}$, (mW) B	$P_{V=775}$, (mW) A	$\Delta P_{V=775}$, (%)	I_{sc}, (mA) B	I_{sc}, (mA) A	ΔI_{sc}, (%)
994	1000.0	990.4	-0.96	78.28	74.87	-4.63	108.0	105.9	-1.94
879	980.8	838.4	-14.52	78.90	14.49	-81.63	108.0	74.0	-31.48
982	995.2	987.2	-0.80	79.67	75.95	-4.66	110.4	105.9	-4.08
971	1009.6	979.2	-3.01	79.83	0	100.00	115.0	29.1	-74.70
877	1004.8	1003.2	-0.16	78.59	78.59	0	107.2	107.8	+0.56
941	974.4	982.4	+0.82	79.67	79.67	0	108.8	109.0	+0.18
Average 1	994.1	963.5	-3.08	79.16	53.93	-31.87	109.6	88.6	-19.16
Average 2*	993.6	990.8	-0.28	79.05	77.27	-2.25	108.6	107.2	-1.29

Note: B = Before, A = After.
*Average 2 disregards cell numbers 879 and 971.

Of the six cells tested two degraded significantly. However, the cause of degradation of both was very readily attributed to an insufficient cleaning process during fabrication. The four remaining cells showed average changes and ranges as follows:

$\Delta_{av} V_{oc}$ = -0.28% (range: -0.96 to +0.82%)

$\Delta_{av} I_{sc}$ = -1.29% (range: -4.08 to +0.56%)

$\Delta_{av} P_{v = 0.775}$ = -2.25% (range: -4.66 to 0.0%)

Here, as before, the accuracy of the figures is ±1.0 percent.

6.3 High Temperature Contacts. Several preliminary studies have been made on the GaAs cells to determine their environmental stability. Improvements have been achieved in their resistance to common environmental agents such as oxygen and water vapor, both at room temperature and under controlled cycles.

One of the major problems with the (AlGa)As-GaAs solar cell is the susceptibility of the (AlGa)As window layer to attack by oxygen and water vapor normally present in air. However, by controlling the conditions during the growth of the layer, the stability of the layers has been greatly enhanced. The major requirement is the absence of all oxygen and water vapor in the growth ambient during epitaxy. Under these conditions a dry, sintered type layer is grown which acts like sintered aluminum oxide in its ability to withstand corrosion.

Cells grown incorporating these steps have been subjected in vacuum to temperatures from 260°C for 16 hours to 400°C for 100 seconds. Both AuZn and AgZn metallized cells were so tested. These cells had AR coatings of Ta_2O_5 but no cover glasses. In preliminary runs it was found that the cover glass adhesive combination could not be used reliably at these temperatures. The cells tested are shown in Table 18. Figures 16 and 17 show typical photo I-V characteristics before and after such testing.

TABLE 18. (A1Ga) As-GaAs SOLAR CELLS* FOR HIGH TEMPERATURE TESTS

Cell	P-Contact**	(A1Ga) As thickness, (μm)	Junction depth, X_j (μm)
2126, 2127 2129, 2132, 2133	AuZn	0.5	0.5
Ag 1, Ag 3, Ag 4	AgZn	1.0	0.9

*AR coating; Ta_2O_5; no glass cover.
**All cells have AuGeNi back contacts on n side.

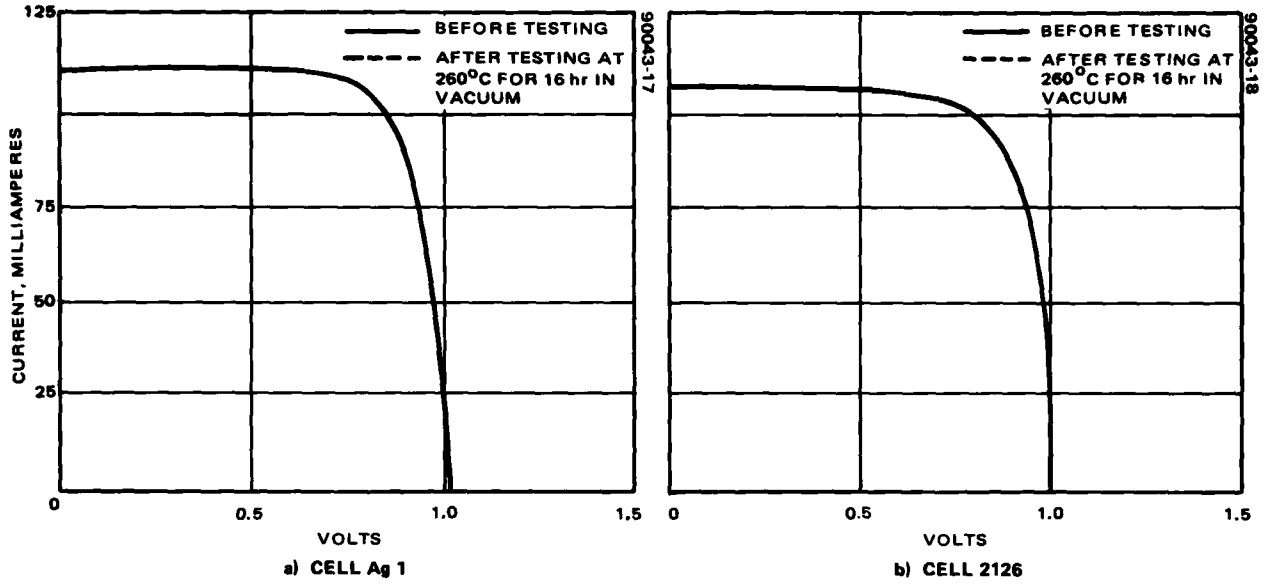

Figure 16. Photo I-V characteristics for test A.

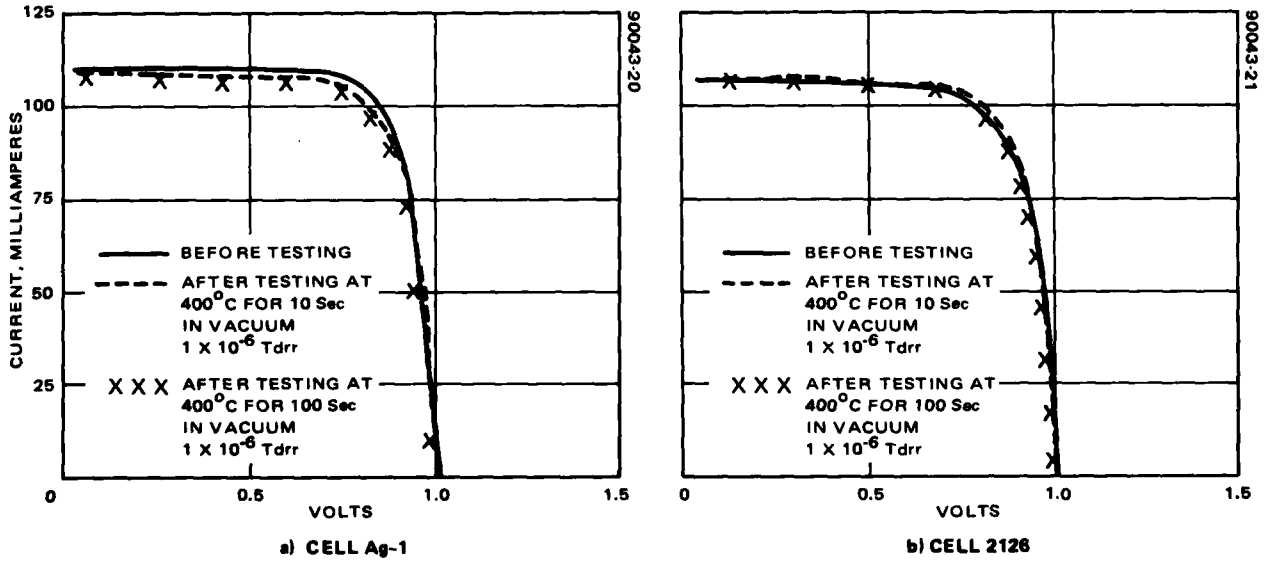

Figure 17. Photo I-V characteristics for test B.

1) Test A: 260°C for 16 hours at 1 x 10^{-6} Torr

Results indicate that there is no degradation of the cells' performance under these conditions. Figure 16 exhibits typical I-V curves for only one AuZn and one AgZn cell respectively. However, all other characteristics for cells in Table 18 were similar.

2) Test B: 400°C for 10 seconds of 1 x 10^{-6} Torr

After the 16 hour test at 260°C in vacuum, these same cells were subjected to a higher temperature test at 400°C for 10 seconds in vacuum. Figure 18 gives the heating and cooling cycle during the test. Figure 17 shows typical photo I-V characteristics before and after the 400°C, 10 second test. Again, there is no sign of degradation.

3) Test C: 400°C for 100 seconds at 1 x 10^{-6} Torr

Again, these same cells were further tested at 400°C for 100 seconds in vacuum. The heating and cooling cycle was kept approximately the same as in Figure 18. Figure 17 also shows the typical photo I-V characteristics before and after the test. These cells once again stood up quite well under this high temperature treatment.

4) Summary

Eight (AlGa)As-GaAs solar cells were subjected to high temperature tests at 260°C and 400°C in vacuum (1 x 10^{-6} Torr). Both front and back contacts survived the tests satisfactorily, and there was no difference in performance between the front AgZn and AuZn metal contacts at these temperatures. In addition, this experiment showed that the (AlGa)As-GaAs solar cells can survive temperature cycling from room temperature to 400°C in vacuum since the present study involved three such cycles. The experimental photo I-V characteristics of a GaAs solar cell as a function of temperatures ranging from -103 to +300°C were plotted. Results are shown in Figure 19.

6.4 Radiation Tests. The radiation hardness of the GaAs cell is of critical importance to the longevity of the cell in any space mission. Consequently, the Hughes GaAs cell has been designed to improve the radiation damage resistance. Prior work revealed that one of the factors that has a controlling influence on the radiation hardness is the junction depth (i.e., the distance of the homojunction from the window layer). The epitaxial growth schedule for the (AlGa)As window layer has been tailored to produce a junction depth of 0.5 μm.

The junction depth is controlled by the temperature at which growth is initiated and by the time for which the growing layer is in contact with the solution. The curves in Figure 20 substantiate the fact that the diffusion rate of Be in the first few minutes after start of growth is the important period determining junction depth. Subsequent diffusion, presumably from the

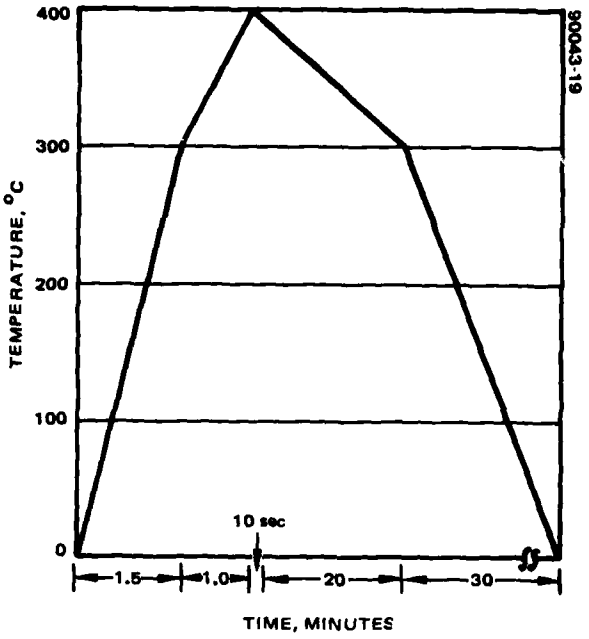

Figure 18. Heating and cooling cycle for (AlGa) As-Ga-As solar cell high temperature tests.

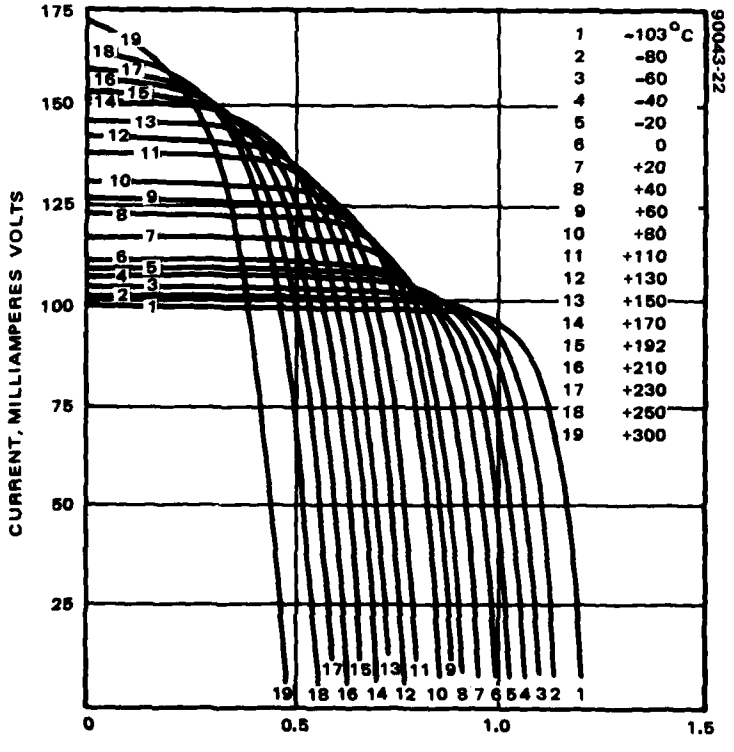

Figure 19. Photo I-V characteristics of cell 2373 as function of temperature.

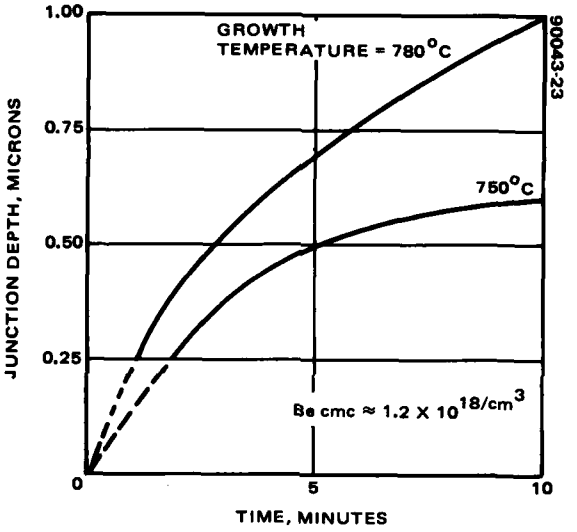

Figure 20. Junction depth versus growth time.

growing layer, is considerably slower. Prior to the present program, a growth temperature close to 800°C had been used for the window layer. However, the junction depth occasionally varied to 0.6 μm, probably because of some differences in Be concentration and substrate characteristics that can slightly affect the nucleation and initial growth. To eliminate such random variability in junction depth control, a careful study of growth temperatures below 800°C was executed. From the results it was concluded that a junction depth of 0.5 μm can be achieved by using a growth temperature of 750°C and a cooling rate that would enable the growth of a window layer approximately 0.5 μm thick in 3 to 4 minutes. The cells shown in Table 19 were grown according to this schedule and the measurements show that the junction depth is acceptable. The HESP II qualifying cells will be grown according to these guidelines.

TABLE 19. (A1Ga) As-GaAs SOLAR CELLS GROWN AT 750°C*

Cell	I_{sc}, (mA)	V_{oc}, (V)	FF	η, (%)
2697	118	1.01	0.75	16.5
2698	117	1.01	0.76	16.5
2699	114	1.01	0.76	16
2700	116	1.01	0.76	16.4
2701	119	1.0	0.75	16.5

*For 3 minutes.

All aspects of preliminary radiation tests for HESP II GaAs solar cells have been addressed in an investigation conducted by Hughes Research Laboratories. Rather than repeat data out of context in this subsection, the presentation is offered in full as the Appendix of this report.

6.5 Welding Tests. In Section 4.3 the ultimate mechanical strength of ultrasonic seam welds was shown to vary with four interdependent parameters: F_C, P, T, and V. As a result, extensive preliminary testing was required to determine the most suitable balance of parameters to effect the most acceptable bond while taking into account operational ease. Once this schedule of parameters was perfected, subsequent welds were subjected to three separate tests: mechanical, electrical, and microscopic.

Mechanical Tests. After welding, the tabs described in Figure 8 were separated and individually destructively pulled at a 45 degree angle. Cells and each of their tabs were indexed for future reference and saved for possible further experimentation. In addition to an identification number and the pull force (in either grams or pounds), the weld condition and that of the metal area beneath the weld (after pulling) were tabulated for each cell. An explanation of the codes adopted and their significance is as follows:

1) AO – Already Off. The weld was a total failure in that the tab did not adhere and was not available for pulling. AO always implies a pull force of zero.

2) TO — Tab Off. During testing, the entire tab (the parts on both sides of the weld area) became totally dislodged. TO indicates a successful weld only for pulls ≥0.50 pound. For strengths less than this, TO implies:

Weld failure — if the metal under the weld area is completely intact. In this case an entry of "1" is made under metal condition.

Metal failure — if the metal under the weld area is less than completely intact. Here "0" is assigned for the metal condition.

3) BAW — Broke At Weld. During testing the tab broke at the weld so that the pulled section was removed while the other portion remained. BAW indicates a successful weld only for pulls ≥0.50 pound. For strengths less than this, BAW implies a weld failure, most likely due to excessive wheel force causing extraordinary deformation of the metals.

4) TB — Tab Broke. During testing the tab itself broke. This may happen either because the weld was excessively strong or because there was a defect in the tab before pulling. Therefore, by means of the associated pull force, TB can indicate an exceptionally good weld. On the other hand, it can never imply anything negative about the weld or metal conditions.

Typical results for the AuZn p type metallization and the AuNiGe n type contact are shown in Table 20. As can be seen, bond strengths for both surfaces exceed 1.0 pound (453.6 grams = 1.0 pound), and values are consistent. Also, welds tend to break at the weld (BAW under weld condition) and the metallizations tend to adhere well (1 under metal condition).

TABLE 20. TYPICAL GaAs CELL TAB PULL RESULTS, CELL 2351

Front contact				Back contact			
Tab	Pull force (gm.)	Weld condition	Metal condition	Tab	Pull force (gm.)	Weld condition	Metal condition
1	544.3	TO	1	1	657.7	TO	0
2	612.3	BAW	1	2	657.7	BAW	1
3	589.7	BAW	1	3	521.6	BAW	1
4	476.3	TO	1	4	385.6	BAW	1
5	498.9	BAW	1	5	567.0	BAW	1
6	476.3	BAW	1	6	635.0	BAW	1

NOTE: F_c = 300 gm., P = 5, V = 48, T = 7.

In Figure 21a and b a distribution in pull strength versus number of tabs pulled for the AuZn system is presented. As can be seen, the mechanical strengths of both upper and lower contacts roughly exhibit bell curves peaking above 1.0 pound.

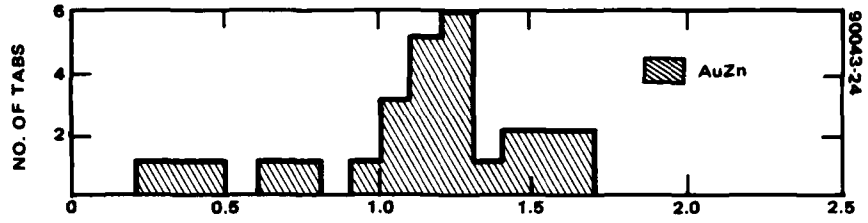

a) AuZn FRONT CONTACT

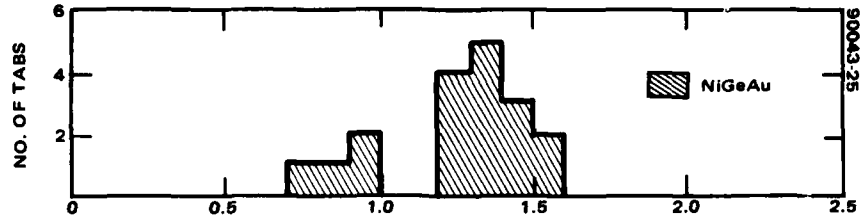

b) NiGeAu BACK CONTACT

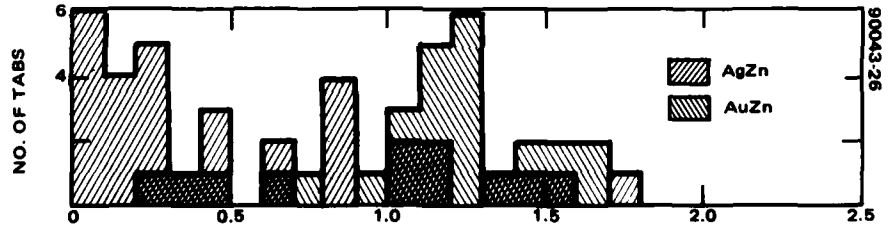

c) AgZn FRONT CONTACT

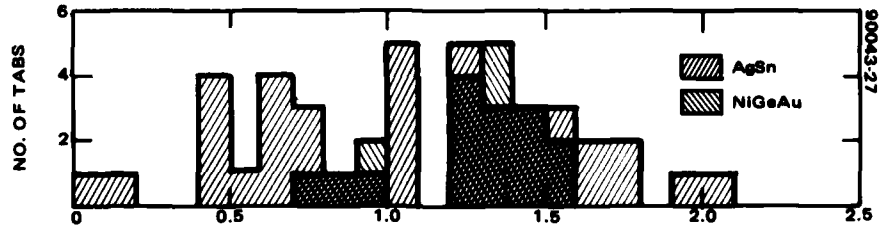

d) AgSn BACK CONTACT

Figure 21. Distribution of pull strengths versus number of tabs pulled.

Significantly, few tabs exhibit relatively weak bonds (<0.5 pound) and none fail entirely.

For comparison purposes, the pull strengths and pull strength distribution of the AgZn (p type) and AgSn (n type) contact systems are superimposed on the same data to produce Figures 21c and d. In general, it can be seen that the average pull strength of welded tabs for the AgSn contact was roughly the same as for NiGeAu, although the distribution is considerably wider. On the other hand, strengths for AgZn were notably inferior to those for AuZn. It must be noted, however, that the study of this metallization system was far from exhaustive, and it is believed that AgZn/AgSn results would improve considerably with experimentation of the deposition process if more time was available. However, the results do confirm the conviction that, at present, AuZn/NiGeAu is considerably superior and was the proper choice for the GaAs metallization.

Electrical Tests. Before and after ultrasonically seam welding tabs to GaAs cells, current voltage characteristics were examined for a number of cells. The majority of cells showed no change whatsoever as shown in Figure 22a. However, occasionally a characteristic was observed to exhibit some minor shunting of the junction as shown in Figure 22b.

Scanning Electron Microscopy Study. A detailed SEM study of the exact nature of the weld was also conducted. Three mechanisms were considered:

1) Purely thermal union (in which metal materials intermingle due to melting)

2) Purely mechanical union (in which metal surface areas become abraded and the resulting fractured surfaces become interlocked)

3) Purely metallurgical union (in which oxides are abraded away so that a metallurgical bond is created between the two clean metal surfaces)

(In practice, a combination of more than one of the above is feasible.)

Extensive SEM studies supported the metallurgical mechanism. In other words, no evidence of melting nor interlocking was observed. Such a welding study is significant in that metals showing metallurgical bonding can be expected to be less prone to failure induced by either temperature cycling or mechanical vibration.

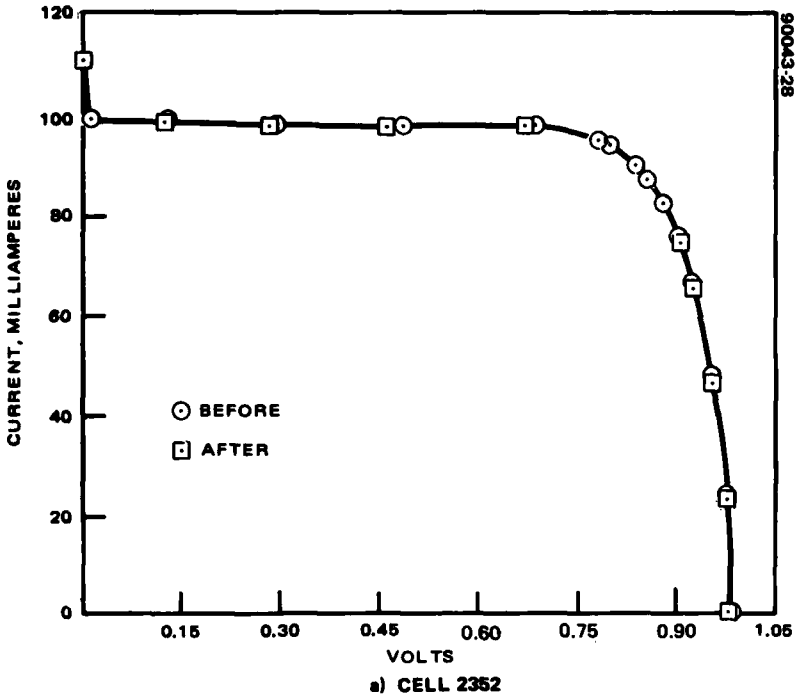

a) CELL 2352

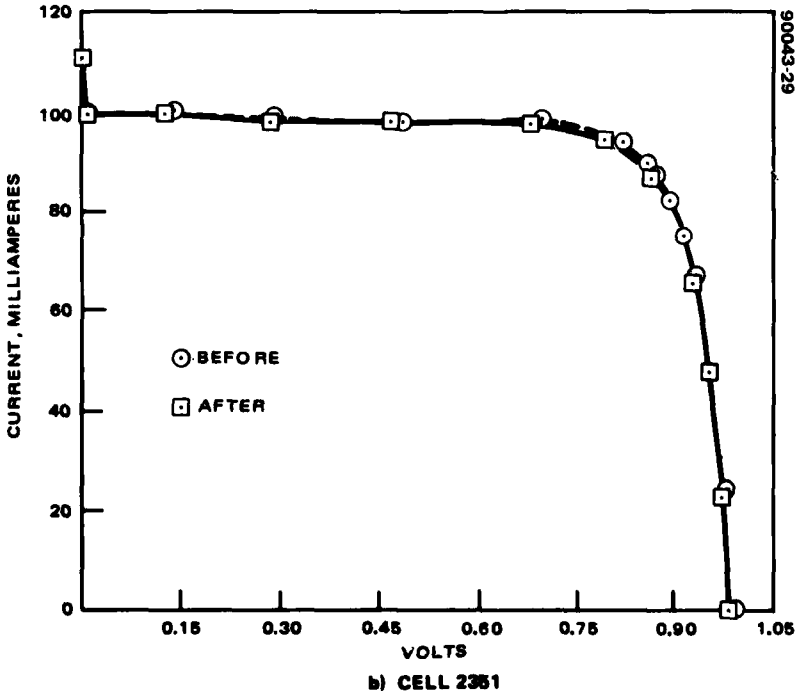

b) CELL 2351

Figure 22. Photo I-V characteristics before and after welding.

7. CONCLUSIONS

7.1 Present Activity. With completion of the testing described in the last section, the development phase of GaAs HESP II has drawn to a close, and manufacturing control documentation and qualification testing has begun.

7.1.1 Manufacturing Control Documentation. Manufacturing control documentation (MCD) is the written record of every detail of the fabrication process. It effectively breaks down complex research operations into relatively simpler steps capable of being followed with relative ease on a production basis at a manufacturing facility. Implicit with the manufacturing control documentation stage of the contract is the cessation of all further research and development and the selection of optimized processes. As such it freezes the cell processing and prevents subsequent changes. This ensures that all cells produced after MCD have nearly identical histories, and therefore, ideally, close to identical performance.

Since the MCD process allows for the manufacture of well-defined, controllable GaAs solar cells as close to identical as possible, the stage is set for qualification testing of such cells in order to determine the ultimate behavior of cells made with the same documentation but under a separate manufacturing facility.

The manufacturing control documentation is expected to be performed in two stages. The intermediate or interim MCD consists of the complete recorded description of all research processes which then goes to the manufacturing facility (Spectrolab). The final MCD is delivered by Spectrolab to the customer as required at the end of the contract.

7.1.2 Qualification Testing. With the manufacturing control documentation underway, qualification testing is imminent. Figure 23 presents the test outline. As can be seen, five major groups of tests are involved:

1) Contact Welding and Temperature Cycling

2) Charged Particle Radiation Resistance

3) Contact Integrity After Welding

4) High Temperature Vacuum and Humidity

5) Electrical Before Glassing and Radiometric Properties

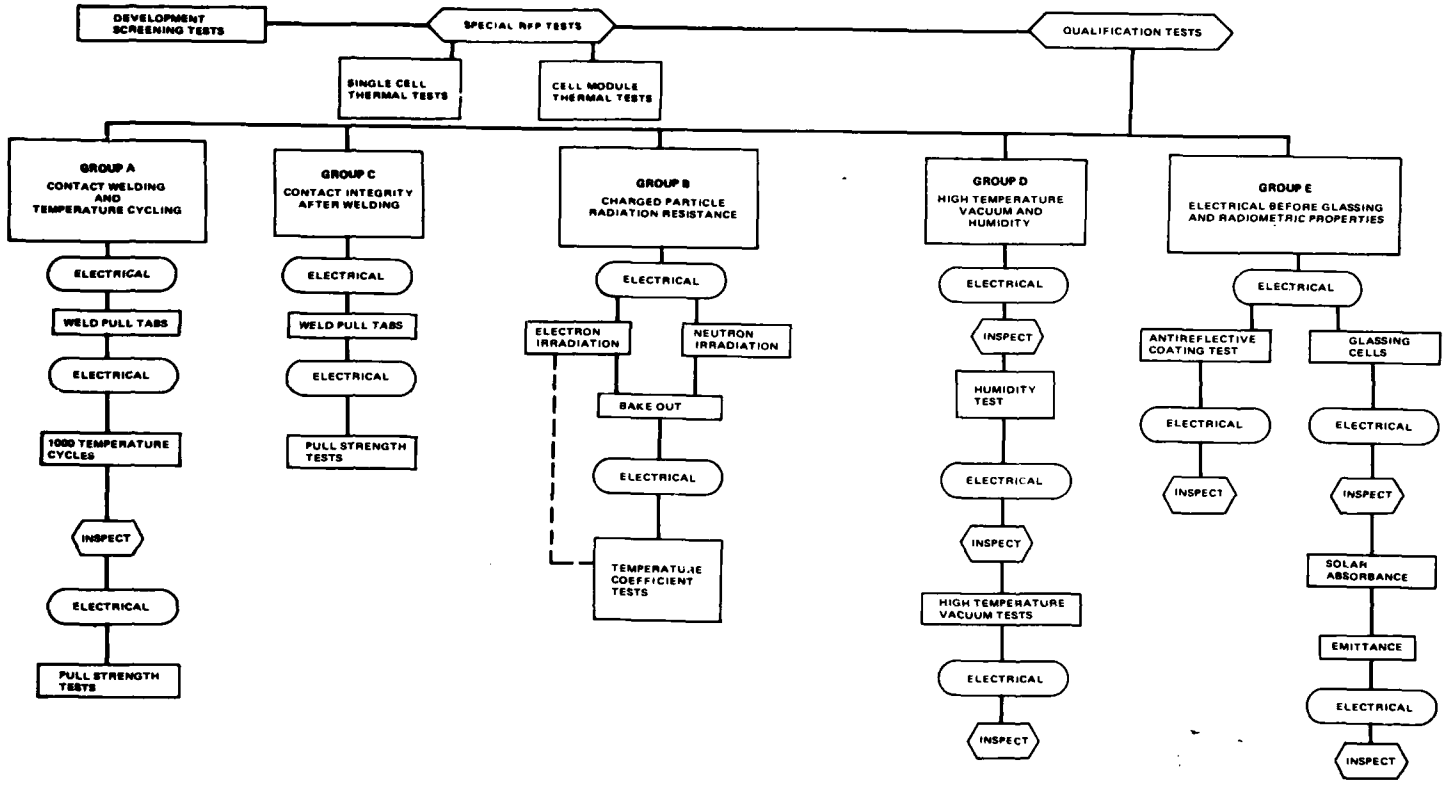

Figure 23. GaAs HESP II qualification test plan.

Details with respect to exact procedures, equipment, personnel, costing, and scheduling with the various groups involved in subtasks of the above are presently being negotiated.

7.2 Accomplishments. To review, the primary goals of the HESP II contract are to produce regularly a 16 percent efficient GaAs solar cell and to establish the most production ready processes. Production ready processes imply those amenable to large scale fabrication using the simplest procedures and incurring the lowest possible costs in both materials and labor. Finally, cells must be radiation hard.

To date 16 percent cells are produced regularly with an excellent yield of ~50 percent. In fact, 17 percent cells are also routinely fabricated at an 18 percent yield, and even 18 percent efficient cells have been demonstrated.

In addition, all developmental research stages of the HESP II program have been completed, resulting in studies of the GaAs substrate, the epitaxial reactors, the LPE growth processes, ohmic contacts, welding compatibility, and environmental testing. Also, large rectangular, 1.0 by 2.0 inch GaAs substrates are regularly supplied, while 2.0 by 2.0 inch and thinner (8.0 mil) substrates are feasible. Experimentation with the LPE reactors and associated epitaxial layers has resulted in the elimination of numerous potential problems such as dopant level, junction depth, and oxidation difficulties and has led to the selection of the most streamlined, production ready processes. In addition, great strides have been made in increasing solution volume and slide bar capability in anticipation of enhanced production capacity. Metallizations for both the upper, p type GaAs surface and the lower, n type have been developed and have proven to be ohmic, low resistance, highly adhesive, and capable of withstanding extreme temperature and humidity environments. Welding studies have been completed, indicating regular production of bond pull strengths exceeding 1.0 pound for each of the twelve individual tabs attached to a single cell. Finally, adequate radiation hardness has been demonstrated.

APPENDIX. RADIATION TEST RESULTS

R. Loo, L. Goldhammer, B. Anspaugh, R. C. Knechtli, and G. S. Kamath, "Electron and Proton Degradation in (AlGa)As-GaAs Solar Cells," 13th Photovoltaic Specialist Conference, June 1978.

ELECTRON AND PROTON DEGRADATION IN (AlGa)As-GaAs SOLAR CELLS

R. Loo, L. Goldhammer,* B. Anspaugh,** R.C. Knechtli and G.S. Kamath

Hughes Research Laboratories
Malibu, California 90265

ABSTRACT

Results on radiation damage in (AlGa)As-GaAs solar cells by 1 MeV electron fluences up to 1×10^{16} e/cm^{-2} and by 15, 20, 30 and 40 MeV proton fluences up to 5×10^{11} P cm^{-2} are presented. The damage is compared with data on state-of-the-art silicon cells which were irradiated along with the gallium arsenide cells. We verified experimentally our theoretical expectation that the junction depth has to be kept relatively shallow, to minimize radiation damage. The damage to the GaAs cells as a function of irradiation, is correlated with the change in their spectral response and dark I-V characteristics. The effect of thermal annealing on the (AlGa)As-GaAs solar cells was also investigated. This data is used to predict further avenues of optimization of the GaAs cells.

INTRODUCTION

The behavior of solar cells under radiation environment is of great importance for space application. Previous studies have shown that the (AlGa)As-GaAs solar cells have achieved an efficiency of 18.5% AMO (1) with a radiation resistance equal to or better than that observed in violet silicon cells (2). In this paper, we report the radiation effect on large-area (2 cm x 2 cm) (AlGa)As-GaAs solar cells fabricated at Hughes Research Laboratories (HRL) using the infinite melt liquid phase epitaxial (LPE) growth system. Our best cell to date has an AMO efficiency of 18%, and our improved shallow-junction cells show more radiation resistance than silicon cells.

GaAs has a large optical absorption constant and a short diffusion length; essentially, all the photovoltaic response is close to the GaAs surface. The radiation damage beyond this active region has a negligible effect on cell performance. Consequently, the reduction in the required minority carrier diffusion length and the relative shallowness of the active region are the key factors that can be exploited to make GaAs solar cells more radiation resistant. Data consistent with these observations is presented below.

*Hughes Aircraft Company, El Segundo, California
**J.P.L., Pasadena, California

EXPERIMENTAL

Figure 1 shows the (AlGa)As-GaAs solar cell structure. The n^+ concentration for the substrate is fixed at $> 5 \times 10^{17}$ cm^{-3} with Te as the dopant. The n buffer layer concentration is 1×10^{17} cm^{-3}. (At this doping level, the open-circuit voltage is 1 V.) The thickness of this layer was fixed at 10 μm or more because results indicated that the substrate visibility is minimized at a buffer layer thickness of 10 μm. A thickness less than this is not always sufficient to remove the effect of the substrate on cell performance.

7845-6

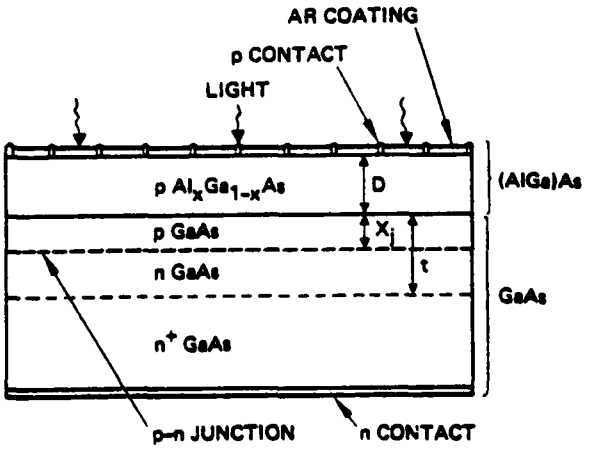

NUMBER OF FINGERS = 24
p CONTACT: Au-Zn-Ag
n CONTACT: Au-Ge-Ni-Ag
AR COATING: Ta_2O_5
p $Al_xGa_{1-x}As$: $X \geq 0.95$
CELL SIZE = 2 x 2 CM^2

Figure 1. The (AlGa)As-GaAs solar cell

The window layer of $(Al_xGa_{1-x})As$ is grown by LPE on GaAs. Our layer has $x > 0.90$, making the bandgap and hence the optical transmission as high as possible. The dopant is beryllium (Be). The concentration is 1×10^{18} cm^{-3}. During (AlGa)As window layer growth, a p-n homojunction is formed by Be diffusion from the (AlGa)As layer into the n buffer layer. The carrier concentration of the p-diffused region is also 1×10^{18} cm^{-3}.

The remaining parts of the baseline structure are self-explanatory. The Au-Zn contacts are about 3000 to 4000 Å with a silver overlay about 4 µm thick, and the n contact is AuGeNi (∿ 5000 Å) with an Ag overlay. The AR coating is Ta_2O_5.

The Dynamitron particle accelerator at JPL was used as the electron source for high-energy electron irradiation; the irradiations were performed in vacuum at room temperature. The uniformity over the test plane was ± 4% with no areas of discontinuity. Fluxes and fluences were measured with a Faraday cup the current of which was integrated to establish electron fluences and to automatically stop the irradiation at the desired fluence levels.

High-energy proton irradiation was performed at the Crocker Nuclear Laboratory at the University of California at Davis. This cyclotron can produce a primary proton beam at energies between approximately 8 and 68 MeV. The solar cells were mounted with small pieces of double-face masking tape to aluminum plates. Each plate was irradiated separately in air at specific proton energies and fluences.* The fluence over the target plane was uniform within ±5%. The cell temperature during irradiation was kept at 30°C.

The full matrix of tests performed on the (AlGa)As-GaAs solar cells and on several representative silicon solar cells are given in Tables 1 and 2.

Table 1. Electron Irradiation Experiments

7545-4

ELECTRON ENERGY MeV	ELECTRON FLUENCE E/CM^2	TYPE AND NUMBER OF CELLS		
		(AlGa)As-GaAs	Si CONVENTIONAL	Si HIGH EFFICIENCY
1.0	1×10^{13}	3	3	3
	4×10^{14}	3	3	3
	1×10^{15}	3	3	3
	5×10^{15}	3	3	3
	1×10^{16}	3	3	3
0.7	1×10^{15}	2		
1.9	1×10^{15}	2		

Table 2. High-Energy Proton Irradiation Experiments

7545-5

ELECTRON ENERGY MeV	ELECTRON FLUENCE E/CM^2	TYPE AND NUMBER OF CELLS		
		(AlGa)As-GaAs	Si HIGH EFFICIENCY	Si CONVENTIONAL
15.4	5×10^{10}	3	5	4
15.4	5×10^{11}	3	4	4
22	5×10^{10}	3	2	3
22	5×10^{11}	3	2	3
30	5×10^{10}	3	2	3
30	5×10^{11}	3	2	3
40	5×10^{10}	3	2	3
40	5×10^{11}	3	2	3

RESULTS AND DISCUSSION

Electron Damage

A group of cells were fabricated early in the program for electron radiation tests. These cells were designed to have high efficiency with no attempt at optimizing the design parameters to increase radiation hardness. Figure 2 shows the maximum power obtained from the cells plotted against 1 MeV electron radiation fluence. These results were then compared with those for two types of silicon cells as shown in Table 1. This showed the need to improve these early cells for better resistance to electron radiation damage at fluences in excess of 4×10^{14}/cm^2.

Figure 3 shows the spectral response before and after electron irradiation. The results show that in these cells the spectral response in the short wavelength region shows greater damage compared to the longwavelength region. Since the optical absorption coefficient is greater for short wave lengths, most of the absorption in this region will be close to the surface of the cell. The photo generated carriers, therefore, must travel farther to reach the junction than do those generated by longer wavelengths. We suspected from the spectral response of the damaged cells that their junctions had to be relativily deep compared to the minority carrier diffusion length in the damaged layer. Our suspicion was confirmed by the measured junction depth of ≥ 1 µm. These observation led us to examine the influence of the junction depth on radiation damage more carefully.

*By comparing the results from previous solar cells irradiated both in air and in vacuum, we found that the ionized gases in air surrounding the cell during irradiation have no effect on the cells.

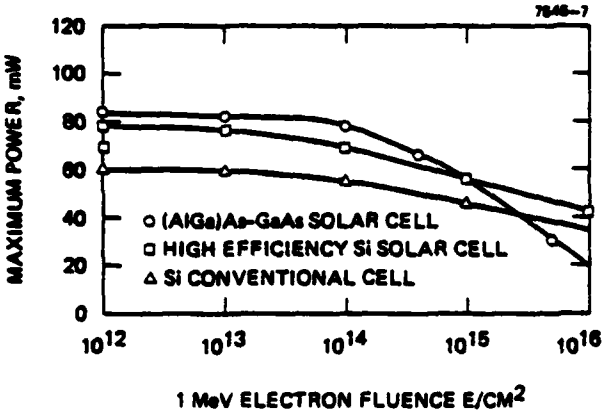

Figure 2. Maximum power as a function of 1 MeV electron fluence

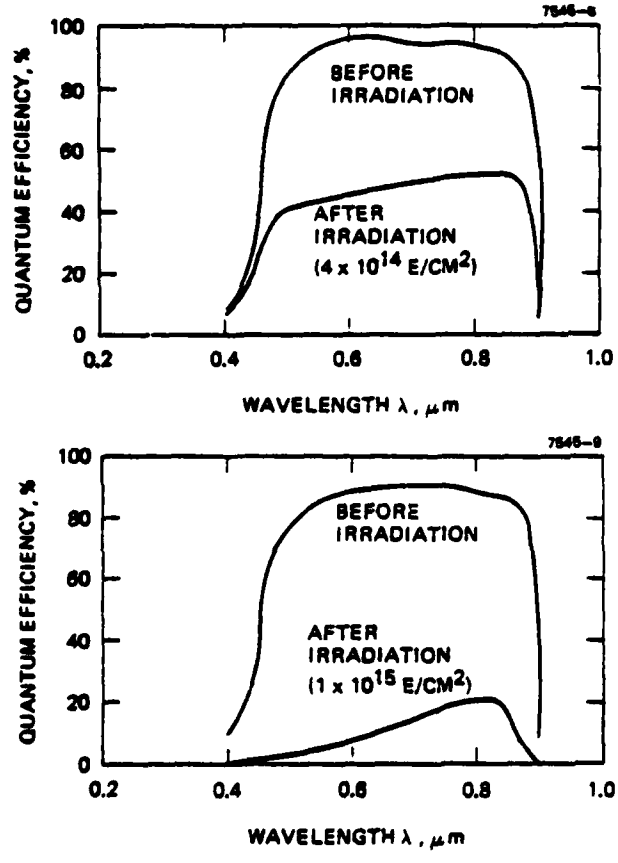

Figure 3. (AlGa)As-GaAs solar cell spectral response before and after 1 MeV electron irradiation

To correlate theory and experiments, Figure 4 shows the (AlGa)As-GaAs solar cell short circuit current density as a function of 1 MeV electron radiation fluence. The continuous curve represents the normalized experimental values. The dotted

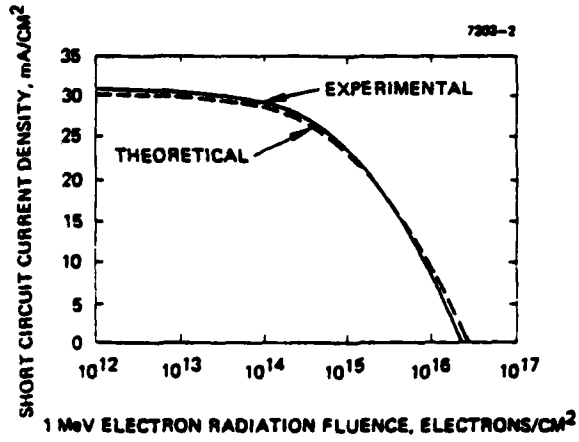

Figure 4. Short circuit current density versus 1 MeV electron radiation fluence, electrons/cm^2

line is the theoretical curve. Both curves correspond to an (AlGa)As layer thickness of 1 μm and a junction depth of 1 μm. For calculating the theoretical curve, the minority carrier diffusion length L was related to the fluence ϕ by the usual relation:

$$\frac{1}{L^2} = \frac{1}{L_o^2} + K_L \phi \ . \qquad (1)$$

The initial diffusion lengths for holes (L_{po}) and electrons (L_{no}) were assumed to be 2 and 5 μm, respectively in these calculations. The damage constant K_L for the diffusion length used for both p- and n-type GaAs was deduced by matching the theoretical curve to the experimental curve as shown in Figure 4. It was found to be $K_L = 7 \times 10^{-8}$, assuming the same value of K_L for the n- and p-doped GaAs.

Using this value for K_L, the short-circuit density was calculated for several junction depths as a function of a 1 MeV electron fluence. The results, shown in Figure 5, show that radiation damage decreases as junction depth decreases.

Based on this analysis, we proceeded to fabricate a second-generation of (AlGa)As-GaAs solar cells with the goal of decreased sensitivity to the radiation environment. The window layer thickness was made at 0.5 μm while the junction depth was decreased to ∿ 0.5 um by readjusting the LPE layer growth parameters.

Figure 6 shows the measured short-circuit current of these shallower junction cells versus 1 MeV electron fluence. The experimentally observed improved radiation resistance is in good agreement

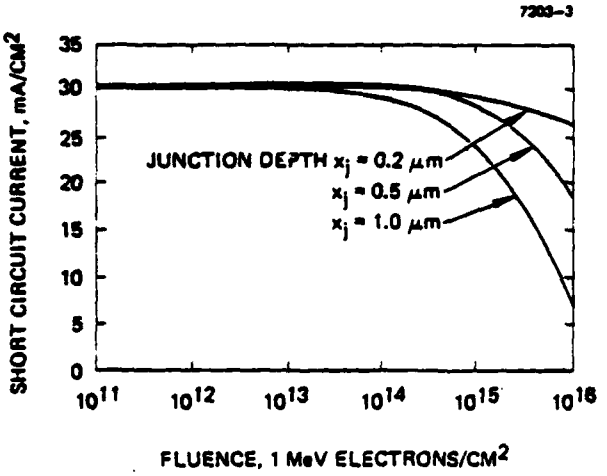

Figure 5. Predicted (AlGa)As-GaAs solar cell short circuit current density versus 1 MeV electron radiation fluence ((AlGa)As layer thickness = 1.0 μm, initial diffusion length L_{po} = 2 μm, L_{no} = 5 μm, and diffusion length damage constant $K_L = 7 \times 10^{-8}$)

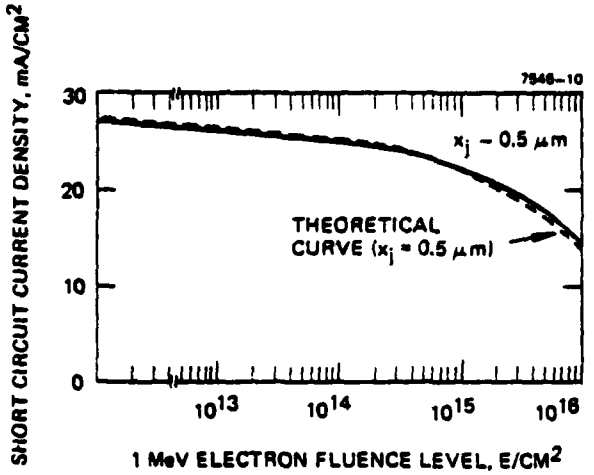

Figure 6. Short circuit current versus electron fluence level (1 MeV)

with the predictions of the theory. Figure 7 shows the experimental results for both (AlGa)As-GaAs solar cells and newly developed high-efficiency Si solar cells as a function of 1 MeV electron irradiation. Also shown for reference are the results of our previous set of irradiated (AlGa)As-GaAs deep-junction solar cells.

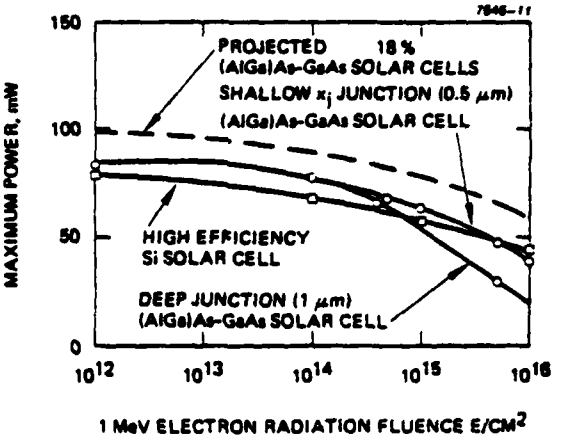

Figure 7. Maximum output power versus 1 MeV electron fluence

The spectral response of the deep-junction and shallower junction cells, both before and after irradiation, are given in Figure 8(a and b). The figure shows that the radiation damage in the deeper junction cells is concentrated in the short-wavelength region, whereas the shallower junction causes the damage to shift to the longer wavelength. This is consistent with our observation that the collection of minority carriers in the p region is not much affected up to the fluence at which the electron diffusion length is reduced to less than the p layer thickness.

Figure 8(c) shows the spectral response of the shallower junction solar cells irradiated at fluences 1×10^{15} e/cm² with electron energies varying from 0.7 MeV to 1.9 MeV. As expected at higher energies, these cells show more degradation, probably because K_L increases with increasing electron energy. Figure 9 shows typical dark current-voltage (I-V) characteristics before and after electron irradiation. Although solar cells become more leaky after irradiation, the basic transport mechanism remains the same (as shown by the I-V curves, which remain parallel to each other). This increased leakage current probably results from an increase in the number of recombination centers at the junction.

High Energy Proton Damage

Twenty-four (AlGa)As-GaAs solar cells and several representative silicon cells were irradiated with 15.4 MeV to 40 MeV protons at fluences of 5×10^{10} and 5×10^{11} p/cm² (Table 2).

The baseline structure of the solar cell used for proton irradiation was the same as that of the shallow-junction solar cells used for electron

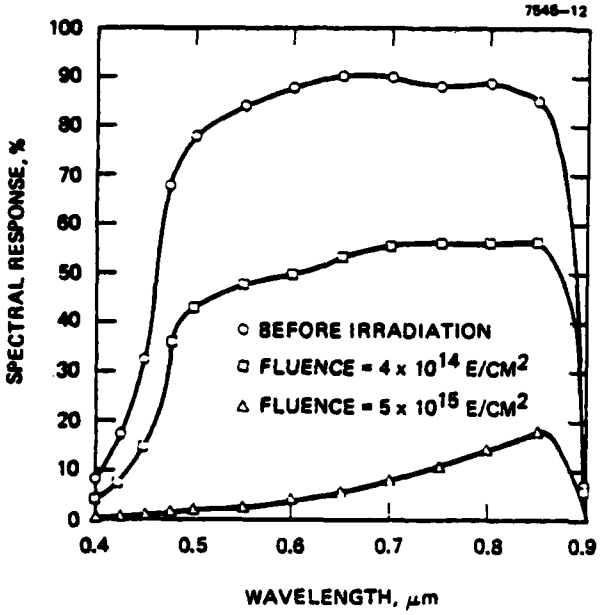

Figure 8(a). (AlGa)As-GaAs solar cell spectral response versus 1 MeV electron radiation fluences

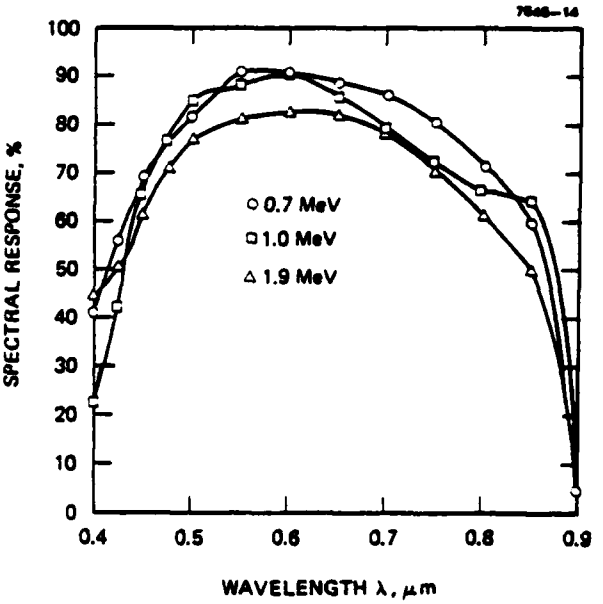

Figure 8(c). (AlGa)As-GaAs solar cell spectral response for several electron energies

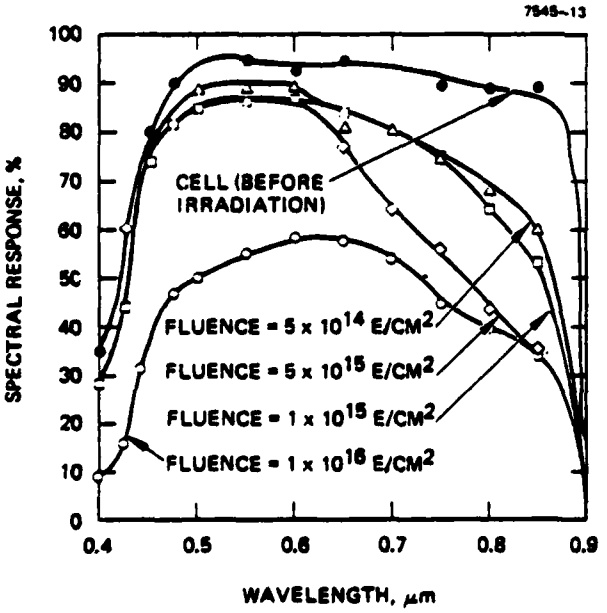

Figure 8(b). (AlGa)As-GaAs solar cell spectral response versus 1 MeV electron radiation fluence

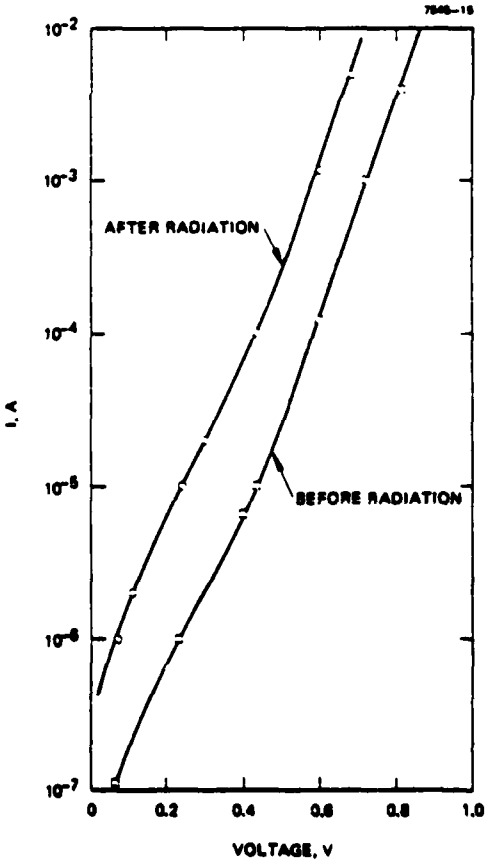

Figure 9. Dark I-V characteristics before and and after electron irradiation

irradiation, except that no cover glass was applied to these cells.

The results of these proton irradiation tests are summarized in Figure 10 (a and b), which shows the maximum solar cell output power versus proton irradiation fluence for the three types of cells specified in Table 2. The (AlGA)As-GaAs solar cells are more resistant to high-energy proton radiation damage than the silicon cells. The dotted lines plotted in Figure 10 are extrapolations of our test results; these show the effect expected from proton fluence on an improved (AlGa)As-GaAs solar cell with a beginning-of-life AMO power-conversion efficiency of 18%. This extrapolation is pertinent since the feasibility of an 18% efficiency has already been demonstrated for this type of cell.

Figures 11 and 12 show the average spectral response of the (AlGa)As-GaAs solar cells before and after proton irradiation with proton energies of 15.4 MeV and 40 MeV, respectively. The spectral response in the short wavelength region of these shallow-junction solar cells is almost insensitive to the proton irradiation. A slight decrease in the solar cell spectral response occurs only in the long wavelength region.

Figure 13 shows the dark I-V characteristic before and after irradiation. Again, just as in the case of electron irradiation, the solar cell junction becomes slightly leaky due to the increasing number of recombination centers produced by proton irradiation although the basic transport mechanism remains unchanged.

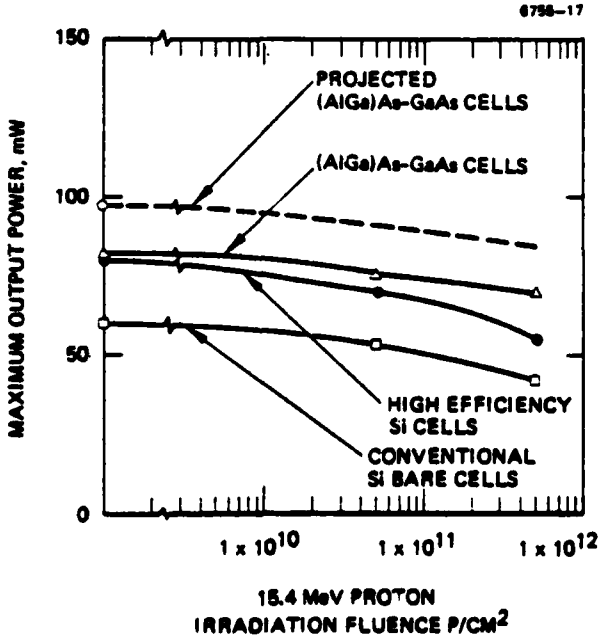

Figure 10(a). Solar cell maximum output power versus 15.4 MeV proton irradiation fluence.

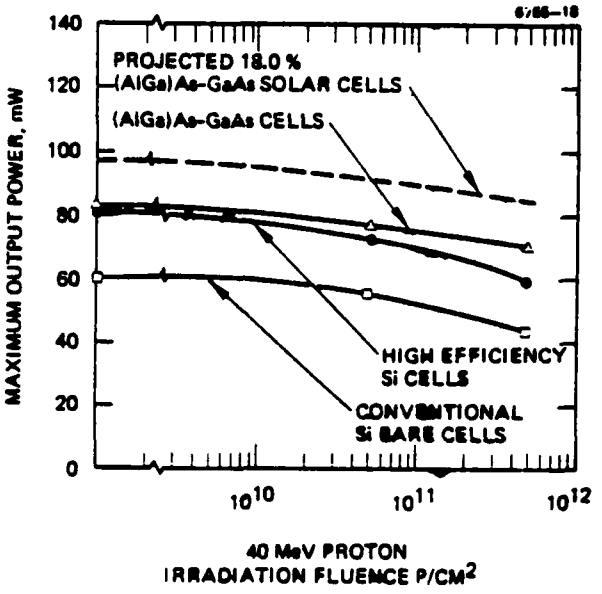

Figure 10(b). Solar cell maximum output power versus 40 MeV proton irradiation fluence

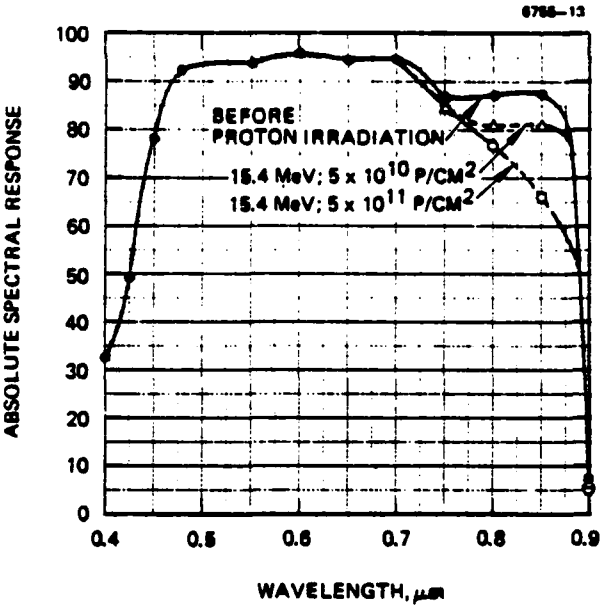

Figure 11. (AlGa)As-GaAs solar cell spectral response before and after 15.4 MeV proton irradiation

Radiation Annealing Studies

GaAs solar cells damaged by radiation recover their efficiency when annealed at low temperatures

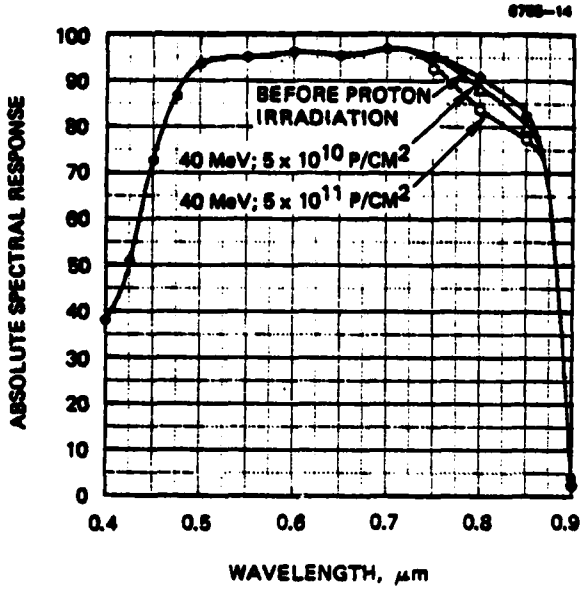

Figure 12. (AlGa)As-GaAs solar cell spectral response before and after 40 MeV proton irradiation

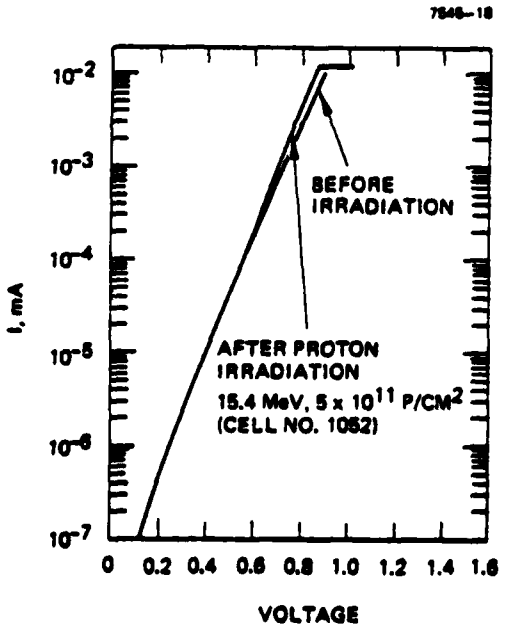

Figure 13. Dark I-V characteristics before and after proton irradiation

Figure 13. Dark I-V characteristics before and after proton irradiation

on the order of 200°C to 300°C (3,4). Some preliminary thermal annealing experiments on the radiation-damaged (AlGa)As-GaAs solar cells were performed in our laboratory. The cells were irradiated at fluences of 1 x 10^{15}/cm^2 with electron energies varying from 0.7 MeV through 1.0 MeV to 1.9 MeV. Subsequently, they were annealed in vacuum at temperatures of over 200°C. Figure 14 shows the effect of annealing as a function of annealing time and temperatures.

Figure 15 compares the spectral response of these cells after the annealing step with the spectral response before and after electron irradiation. The long wavelength region shows significant recovery. This suggests that the annealing leads to a significant recovery in the minority carrier diffusion length in GaAs after radiation damage.

Figure 16 shows the dark I-V characteristics of these cells. These cells show leaky p-n junctions after irradiation; however, they almost completely recover to their pre-irradiation condition after annealing at 210°C. These results indicate that (AlGa)As-GaAs solar cells can be annealed at practical temperatures to remove radiation damage. This could be exploited for longer space missions.

CONCLUSION AND SUMMARY

Several 2 cm x 2 cm (AlGa)As-GaAs cells were subjected to radiation damage studies using both electrons and protons. The results show that:

- (AlGa)As-GaAs solar cells can be made more resistant to radiation damage than can silicon cells for both electron and proton irradiation.
- The junction depth is a sensitive parameter in determining radiation resistance.
- The (AlGa)As-GaAs solar cells suffer only a moderate amount of degradation at proton energies above 15.4 MeV.
- The efficiencies of electron-radiation-damaged (AlGa)As-GaAs solar cells recover when annealed at temperatures as low as 200°C to 300°C.

ACKNOWLEDGMENT

The radiation damage studies reported here were supported in part by contracts from NASA Langley, Contract NAS 1-14727

REFERENCES

1. J.M. Woodall and H.J. Hovel, "An Isothermal Etchback – Regrowth Method for High efficiency GaAlAs-GaAs Solar Cells," Appl. Phys. Lett. 30, 492 (1977).
2. R.I. Moon, et al., "Performance of (AlGa)As-GaAs Solar Cells in the Space Environment," 12th IEEE Photovoltaic Specialists Conference, 255 (1975).
3. R.S. Miller and J.S. Harris, "Gallium Arsenide Concentration System," presented at the AIAA Conference on the Future of Aerospace Power System, March 1977.
4. G.H. Walker and E.J. Conway, "Annealing of GaAs Solar Cells Damaged by Electron Irradiation," J. of Electrical Chemical Society, Vol. 125, No. 4, p. 676, 1978.

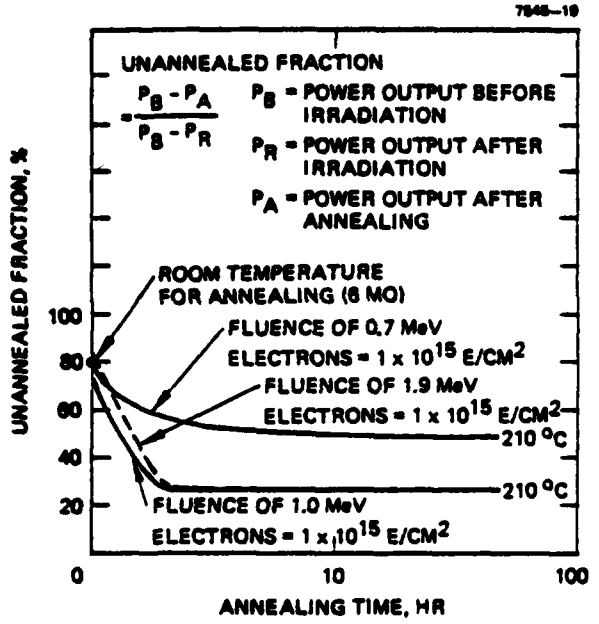

Figure 14. Unannealed fraction versus annealing time

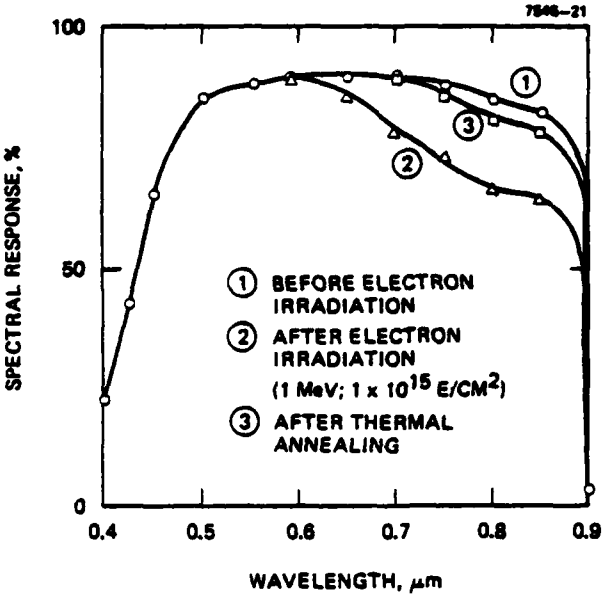

Figure 15(b). Spectral response before and after thermal annealing cell #1008

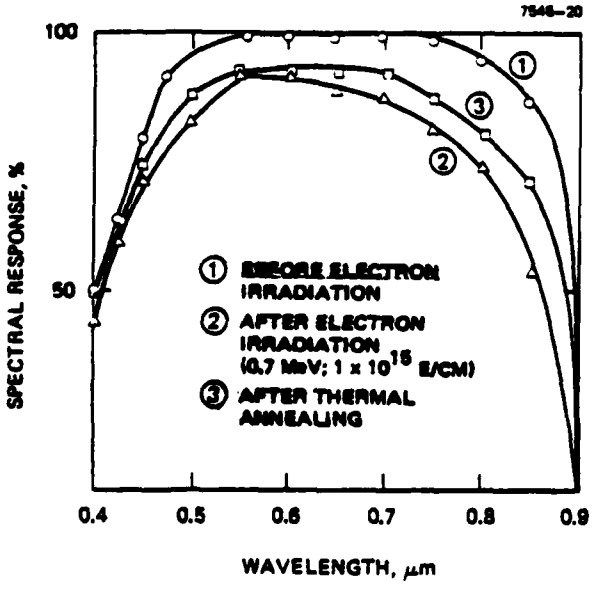

Figure 15(a). Spectral response before and after thermal annealing Cell #1222

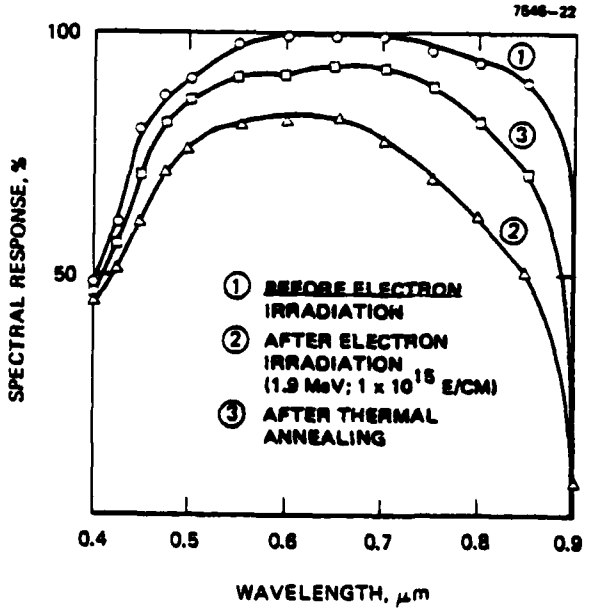

Figure 15(c). Spectral response before and after irradiation and after annealing cell #1278

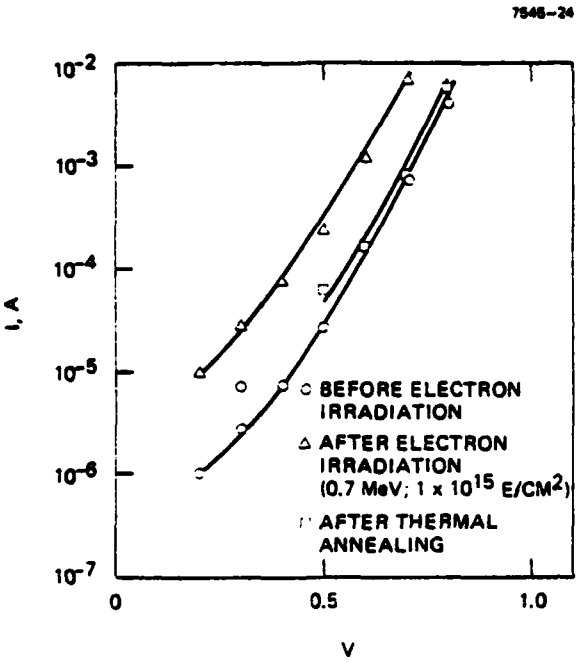

Figure 16(a). Dark I-V characteristic before and after thermal annealing cell #1222

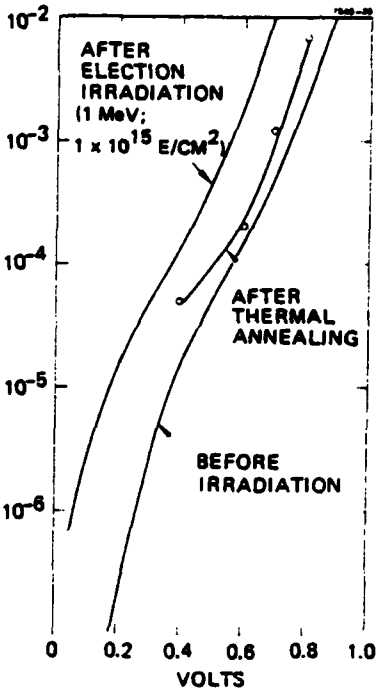

Figure 16(b). Dark I-V characteristic before and after thermal annealing cell #1008

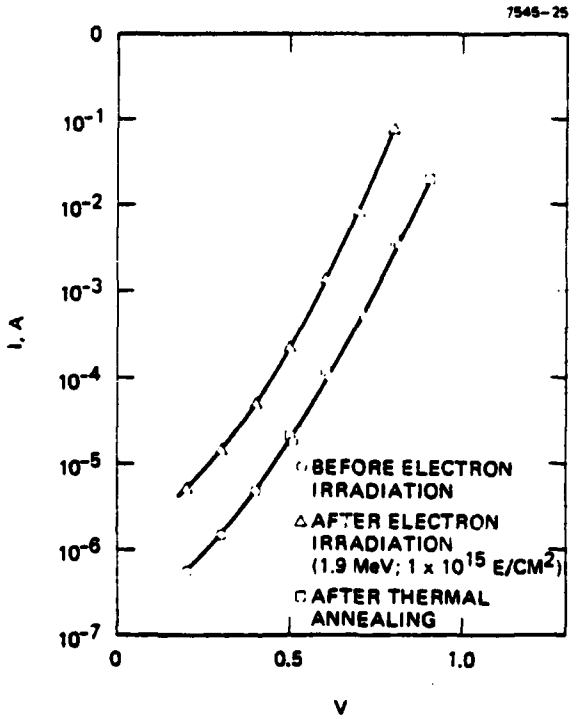

Figure 16(c). Dark I-V characteristic before and after thermal annealing cell #1278

*U.S.Government Printing Office: 1979 — 657-084/347